

## The high sensitivity of stable carbon and oxygen isotopic compositions of peatland *Sphagnum* mosses to seasonality

Zhengyu Xia<sup>a,\*</sup>, Yueyan Jiang<sup>a</sup>, Yingfan Xia<sup>a</sup>, Meng Wang<sup>a</sup>, Shaoqing Zhang<sup>b</sup>, Zhao-Jun Bu<sup>a</sup>, Zicheng Yu<sup>a,c,\*</sup>

<sup>a</sup> Key Laboratory of Geographical Processes and Ecological Security in Changbai Mountains, Ministry of Education, School of Geographical Sciences, Northeast Normal University, Changchun, China

<sup>b</sup> Key Laboratory of Wetland Ecology and Environment, Northeast Institute of Geography and Agroecology, Chinese Academy of Sciences, Changchun, China

<sup>c</sup> State Key Laboratory of Black Soils Conservation and Utilization, Northeast Institute of Geography and Agroecology, Chinese Academy of Sciences, Changchun, China

### ARTICLE INFO

Editor: Bing Shen

**Keywords:**

Peatlands  
*Sphagnum* mosses  
Carbon isotopes  
Oxygen isotopes  
Modern processes

### ABSTRACT

The stable carbon ( $\delta^{13}\text{C}$ ) and oxygen ( $\delta^{18}\text{O}$ ) isotopic compositions of *Sphagnum* mosses are paleoenvironmental proxies in peatland archives. However, our understanding of the environmental controls on isotopic proxies is largely based on space-for-time substitution and remains incomplete due to the lack of studies that characterize the nature of temporal variability on seasonal and inter-annual timescales. Here, we present a unique dataset of *Sphagnum* cellulose  $\delta^{13}\text{C}$  and  $\delta^{18}\text{O}$  measurements that capture the full ranges of both spatial variations across local microtopographic gradients and temporal variations at sub-annual resolution from a peatland in Northeast China. The spatial dataset, derived from surface *Sphagnum* mosses, supports the “water film” effect on the  $\delta^{13}\text{C}$  signal and the evaporative enrichment effect on the  $\delta^{18}\text{O}$  signal that have been established in previous studies. The temporal dataset, derived from millimeter-scale sequential analysis of long *Sphagnum* moss shoots, reveals cyclic variations in  $\delta^{13}\text{C}$  and  $\delta^{18}\text{O}$  with magnitudes that are similar to and twice as large as those of the spatial dataset, respectively, and are interpreted as time series of multiple seasonal cycles. There are distinguishable changes in levels or lengths of isotopic peaks and troughs that might be linked to changes in seasonal climate conditions but the patterns differ between locally contrasting habitats. Our results highlight the previously unrecognized high sensitivity of *Sphagnum*  $\delta^{13}\text{C}$  and  $\delta^{18}\text{O}$  signatures in growth increments to seasonality, implying that changes in seasonal climate and *Sphagnum* growth patterns may affect the “mean-state”  $\delta^{13}\text{C}$  and  $\delta^{18}\text{O}$  values preserved in peatland records and should be considered in proxy interpretations.

### 1. Introduction

Peatlands are widespread carbon-rich ecosystems and terrestrial archives for past climate variability, despite only occupying 3–4 % of the planet’s land surface (UNEP, 2022). For decades, a range of temperature- or moisture-related proxies have been developed, calibrated, and applied to peatland archives for paleoenvironmental reconstructions on timescales mostly within the Holocene (Chambers et al., 2012). These paleo-records are highly valuable for understanding spatiotemporal patterns, dynamics, and mechanisms of past climate variability (Barber et al., 2003; Turney et al., 2004; Booth et al., 2006; Xie et al., 2013) and for assessing the trajectories of carbon-rich peatland ecosystems under climate changes and anthropogenic pressures (Huang et al., 2018;

Swindles et al., 2019; Zhang et al., 2020; Garcin et al., 2022).

The stable carbon ( $\delta^{13}\text{C}$ ) and oxygen ( $\delta^{18}\text{O}$ ) isotopic compositions of peat-forming plants are paleoenvironmental proxies increasingly applied to peatland archives (Chambers et al., 2012), thanks to the development and commercialization of mass spectrometers, which make the analysis accessible, rapid, and possible even with very small sample sizes. These isotopic proxies can track the natural processes of isotopic fractionation that accompany the cycling of bio-elements in peat-forming plants and peatland ecosystems and are highly sensitive to environmental changes (Rice, 2000; Amesbury et al., 2015a; Amesbury et al., 2015b; Huang et al., 2018; Shi et al., 2019). In this context, *Sphagnum* mosses are among the most important peat-forming plant as isotopic recorders due to their dominant distribution and good

\* Corresponding authors at: Key Laboratory of Geographical Processes and Ecological Security in Changbai Mountains, Ministry of Education, School of Geographical Sciences, Northeast Normal University, Changchun, China.

E-mail addresses: [zhyxia@hotmail.com](mailto:zhyxia@hotmail.com) (Z. Xia), [yuzc315@nenu.edu.cn](mailto:yuzc315@nenu.edu.cn) (Z. Yu).

preservation in global peatlands (Clymo and Hayward, 1982; Rydin and Jeglum, 2013), as well as their relatively simple physiology (without root and stomata) compared to vascular plants (Rice, 2000; Daley et al., 2010; Xia et al., 2020).

Previous studies—based on analyzing photosynthetic gas exchange characteristics and natural plant tissues across local moisture gradients—suggest that the  $\delta^{13}\text{C}$  signature of *Sphagnum* mosses is primarily controlled by the “water film” effect (Rice and Giles, 1996; Williams and Flanagan, 1996; Price et al., 1997; Loisel et al., 2009). Briefly, a passively variable water layer causes a major limitation to  $\text{CO}_2$  diffusion in mosses. With higher water content, the turnover rate of  $\text{CO}_2$  around the RuBisCO is slower, resulting in an increased supply and fixation of  $^{13}\text{CO}_2$  and higher  $\delta^{13}\text{C}$  values in photosynthetic products (mostly sucrose; Marschall, 2010) that are then incorporated into synthesized cellulose (Farquhar et al., 1989). Conversely, lower water content results in lower  $\delta^{13}\text{C}$  values in plant tissues, although metabolic slowdown would occur at very low water content (Williams and Flanagan, 1996). Multiple recent studies confirm the water film effect with different approaches, particularly when analyzing *Sphagnum* mosses growing in distinct local-scale microtopographical locations (Brader et al., 2010; Huang et al., 2014; Loader et al., 2016; Granath et al., 2018; Xia et al., 2020; Serk et al., 2021; Royles et al., 2022; Xia et al., 2025). However, some studies also show empirical relationships between  $\delta^{13}\text{C}$  and temperature, with negative correlations across altitudinal transects (Ménot and Burns, 2001; Skrzypek et al., 2007) or positive correlations by manually matching inter-annual variability between peat core-based  $\delta^{13}\text{C}$  records and instrumental climate data within chronological uncertainties (Kaislahti Tillman et al., 2010b; Kaislahti Tillman et al., 2013). Their mechanisms may respectively be related to the co-variation between temperature and water content (Ménot and Burns, 2001) or the theoretical temperature effect on chloroplastic demand (Rice, 2000).

Both observations and mechanistic models agree that the  $\delta^{18}\text{O}$  signature of *Sphagnum* mosses is controlled by (i) peatland source water (mostly precipitation for nutrient-poor species)  $\delta^{18}\text{O}$ , (ii) a component of evaporative enrichment (0–3 %) that increases metabolic leaf water  $\delta^{18}\text{O}$  relative to the source water, and (iii) a near-constant biochemical fractionation of biosynthesis (about 27 %) from sucrose to cellulose (Brenninkmeijer et al., 1982; Ménot-Combes et al., 2002; Zanazzi and Mora, 2005; Loader et al., 2016; Granath et al., 2018; Xia et al., 2020). The fidelity of *Sphagnum*  $\delta^{18}\text{O}$  in tracking the source water  $\delta^{18}\text{O}$  has been strongly demonstrated by their own strong positive correlations derived from a spatial network of ombrotrophic (rain-fed) sites spanning a large climatological gradient of precipitation  $\delta^{18}\text{O}$  (Ménot-Combes et al., 2002; Granath et al., 2018), and also from repeated sampling within a single site in different seasons (Daley et al., 2010; Royles et al., 2022). However, the  $\delta^{18}\text{O}$  signature also varies within a single site, with slightly higher  $\delta^{18}\text{O}$  values in drier hummocks than in wetter hollows (Aravena and Warner, 1992; Ménot-Combes et al., 2002; Loader et al., 2016; Xia and Yu, 2020; Xia et al., 2020; Xia et al., 2025). This local-scale variability has been attributed to variable degrees of evaporative enrichment effect, the magnitude of which is, however, much smaller than that in vascular plants (Brenninkmeijer et al., 1982; Ménot-Combes et al., 2002; Xia and Yu, 2020).

Despite progress in understanding the control of modern variability in *Sphagnum*  $\delta^{13}\text{C}$  and  $\delta^{18}\text{O}$  signatures, isotope-proxy interpretations in peat-based paleoenvironmental reconstructions are inconsistent in the literature. For example, *Sphagnum*  $\delta^{13}\text{C}$  data have been interpreted as temperature or moisture indicators in different studies, even in opposite directions (Nichols et al., 2009; Kaislahti Tillman et al., 2010b; Loisel et al., 2010; Moschen et al., 2011; Kaislahti Tillman et al., 2013). Published *Sphagnum*  $\delta^{18}\text{O}$  records have been thought to reflect changes in precipitation  $\delta^{18}\text{O}$ , but they show marked differences from open-lake and speleothem carbonate  $\delta^{18}\text{O}$  records of the same region (McDermott et al., 2001; Constantin et al., 2007; Daley et al., 2009; Daley et al., 2010; Finkenbinder et al., 2016; Túri et al., 2021), with some being re-interpreted to potentially contain certain changes related

to evaporative enrichment (Finkenbinder et al., 2016; Xia et al., 2020). A shortcoming in existing modern calibration studies arises from the commonly adopted methodology of space-for-time substitution (spatial calibration), which examines the present-day correlation between proxies and environmental conditions (Booth, 2002; Loader et al., 2016; Naafs et al., 2017). However, limited efforts have been made to characterize the nature of temporal variability in *Sphagnum*  $\delta^{13}\text{C}$  and  $\delta^{18}\text{O}$  signatures on seasonal and inter-annual timescales (Daley et al., 2010; Yasuda et al., 2015; Xia et al., 2020; Royles et al., 2022; Xia et al., 2025), leaving our understanding of natural variability in isotopic proxies and their environmental controls incomplete. While peat-based paleoenvironmental reconstructions commonly interpret these isotopic proxies as reflecting “mean growing-season” conditions (Daley et al., 2010; Xia et al., 2018; Loisel et al., 2023), we know very little about the magnitude and sensitivity of seasonal variations in isotopic signals with plant growth in response to changing environmental conditions. It is possible that a consideration of potential seasonal behaviors and biases in these proxies could help reconcile inconsistencies in proxy interpretations.

In this study, we aim to reduce this knowledge gap by collecting a dataset from Hani peatland in Northeast China, which documents both microtopographic and short-term temporal variability of *Sphagnum*  $\delta^{13}\text{C}$  and  $\delta^{18}\text{O}$  signatures. We recognize that our study cannot fully separate or quantify the competing effects of different factors debated in the literature. Our primary motivation is to characterize the little-known but potentially high-resolution, seasonally resolved, temporal variations of  $\delta^{13}\text{C}$  and  $\delta^{18}\text{O}$  contained in dissected growth increments of *Sphagnum* mosses collected from two contrasting peatland habitats, compare their magnitudes against microtopographic variations, and explore whether these can be correlated with instrumental data. Specifically, we use millimeter-scale sequential analysis of long *Sphagnum* moss shoots, an approach previously explored (Loader et al., 2007; Yasuda et al., 2015; Robinson et al., 2018) and recently demonstrated and refined by the authors (Xia et al., 2020; Xia et al., 2025), to generate sub-annual  $\delta^{13}\text{C}$  and  $\delta^{18}\text{O}$  time series spanning the last several years. This analysis uncovers multiple large-magnitude cycles in  $\delta^{13}\text{C}$  and  $\delta^{18}\text{O}$  signatures along moss shoots that can be linked to seasonal changes in environmental conditions. We discuss how this finding provides new insights into isotope-proxy interpretations in peat-based paleoenvironmental reconstructions.

## 2. Materials and methods

### 2.1. Sampling site

Our sampling site is Hani peatland (42.215°N, 126.512°E, 895 m asl) on the western flank of the Changbai Mountains in Northeast China (Fig. 1a). The region has a temperate continental monsoon climate with strong seasonality (Köppen climate type *Dwb*). The mean annual, summer, and winter temperatures are 4 °C, 20 °C, and –14 °C, respectively. The mean annual precipitation is about 750–800 mm, with 80 % concentrated in the summer monsoon season (May–September). These numbers are based on weather station data (from 1981 to 2010) from Jingyu County (550 m asl), about 30 km northeast of Hani peatland. Precipitation in other months is mainly in solid form, with persistent snowpack throughout the winter half-year.

Hani peatland is a temperate, mesotrophic peatland located in a local valley of volcanic terrain and has been under decades of investigations (Hong et al., 2005; Schröder et al., 2007; Zhou et al., 2010; Bu et al., 2011; Wang et al., 2019; Zhang et al., 2019). *Sphagnum* moss-dominated hummocks are widespread across the site, containing species *S. magellanicum* and *S. fuscum* that favor nutrient-poor conditions, although the dominant vegetation of the peatland is sedge and reed. Due to the monsoon climate, the peatland surface is perennially saturated (Zhou et al., 2010). As a site in the headwater catchment, it is fed by a combination of precipitation and surface inflows from surrounding hillslopes (Zhang et al., 1997; Schröder et al., 2007).

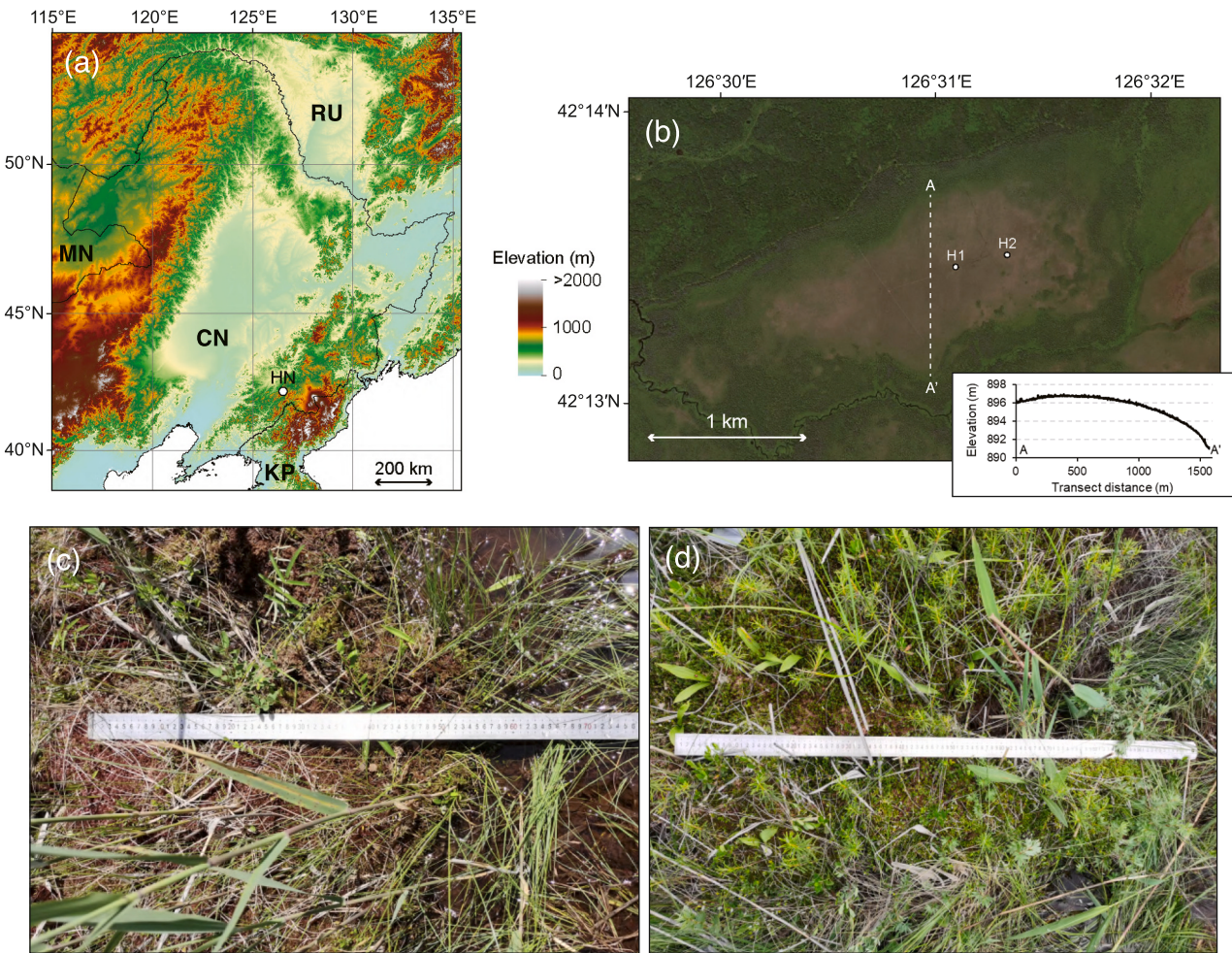


**Fig. 1.** (a) Location of Hani peatland (HN) in Northeast China shown on a map colored for elevation (country names: CN–China, KP–North Korea, RU–Russia, MN–Mongolia). (b) Aerial view of its northern open area marked with specific locations of sampling (H1 and H2). The inset plot shows the drone-based elevation data across the A–A' profile. (c) Microtopographic transect H1 from small hummock to hollow with shallow standing water. (d) Microtopographic transect H2 from large hummock to hollow.

## 2.2. Field sampling

In early July 2022, we conducted fieldwork in the northern open area of Hani peatland and collected two types of contemporary *Sphagnum* moss samples from two hummock microforms. First, we collected surface *Sphagnum* mosses at even distances across two different meter-long local hummock-hollow transects (Fig. 1b). One transect is located on a relatively moist, small hummock (H1) dominated by *S. magellanicum*, with sedge and reed present (Fig. 1c). The other transect is located on a relatively dry, large hummock (H2) dominated by *S. palustre*, *S. fuscum*, and *Polytrichum strictum*, with more dry-adapted low shrubs (Fig. 1d). These two hummocks are located at slightly raised locations with the peatland, shown in a drone-based elevation survey (Fig. 1b), and are very likely associated with local ombrotrophy. The hollows adjacent to these two hummocks contained shallow standing water on the surface at the time of sampling (Fig. 1c and d). We harvested these surface *Sphagnum* mosses with a serrated knife every 5 cm at H1 and 20 cm at H2 along their transects. We further cut them to retain only the top parts, which include capitula and approximately 2-cm stem sections below the capitula, and then immediately placed them into resealable sample bags.

Second, at the hummock-hollow transect H1, we hand-collected the longest possible intact *Sphagnum* mosses—we refer to these as “long shoot” samples, which we aim to use as recorders of environmental conditions during their recent growth, analogous to tree rings. A 28-cm-

long shoot of *S. magellanicum* was collected from the surrounding edge of the hummock (Fig. 2a). There, *Sphagnum* mosses appear to grow horizontally, and such long shoots potentially indicate rapid length increments. Additionally, a 7-cm-long shoot of *S. magellanicum* was collected close to the top of the hummock (Fig. 2b). Further longer shoots were impossible to collect because the shoots were intertwined with each other and had become fragile due to decomposition and compaction. These two long-shoot samples represent typical wet and dry habitats of *Sphagnum* mosses at our site, and there are clear differences in structural and morphological characteristics between these two shoots collected at contrasting microtopographical locations. The shoot from the hummock edge has sparse, more elongated branches along the stem, whereas the shoot from the hummock top is robust with densely distributed branches (Fig. 2a and b).

## 2.3. Sample processing

Back in the laboratory, we first measured the moisture content of the *Sphagnum* mosses in sealed surface samples, expressed as the percentage of water mass to dry mass, following Rydin and McDonald (1985). We then subsampled the surface and long-shoot samples for cellulose extraction.

For surface samples, we cut off the topmost 0.5-cm sections of stems below the capitula using a razor blade under a stereomicroscope and

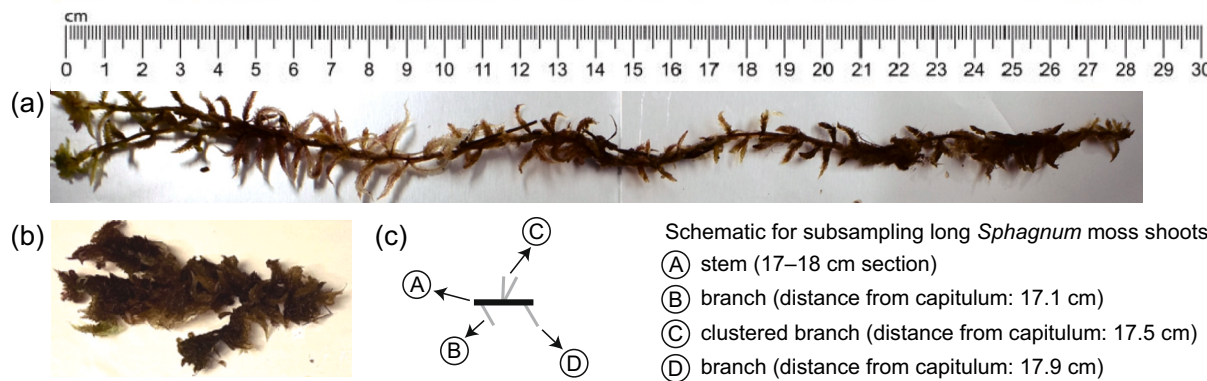


**Fig. 2.** (a) Photo of the 28-cm-long *Sphagnum* shoot collected from the hummock edge. (b) Photo of the 7-cm-long *Sphagnum* shoot collected from the hummock top. Note that bifurcated sections were removed and not analyzed. (c) A schematic drawn to illustrate how we sampled stems (dissected into 1-cm sections) and branches (individually removed from the stem) from long *Sphagnum* moss shoots.

concentrated such material from no fewer than 8 individual shoots of the same species, assuming that these would represent their most recent growth.

For long-shoot samples, we dissected the stem along the moss shoot into 1-cm sections. We also removed all individual branches one by one from the stem and recorded the distance of branches to the capitula. A schematic drawing for subsampling is shown in Fig. 2c. Sometimes, there was a cluster of multiple branches attached to the stem ("C" in Fig. 2c), and the whole cluster was treated as "one branch sample". We did not distinguish hanging and spreading branches, which can be noticeably different among hummock species. For the 28-cm-long shoot, we obtained 27 stem and 97 branch samples. We treated the first centimeter of that moss shoot as the capitulum, consequently resulting in one less stem sample than the length in centimeters. For the 7-cm-long shoot, we obtained 7 stem and 46 branch samples. Using a single moss shoot without combining bifurcations eliminates potentially unparallel isotopic variations (Loader et al., 2007), and including *Sphagnum* branches in the analysis increases our confidence in identifying the seasonal cycles of isotopic variations along the shoots.

We extracted cellulose from these subsamples following the established protocol of the alkaline bleaching method (Loader et al., 1997; Kaislahti Tillman et al., 2010a; Xia et al., 2020). A detailed procedure for cellulose extraction is described in Text S1. If the weight of extracted cellulose was high, about 0.1–0.3 mg of cellulose (depending on the availability of each sample) was enclosed in tin and silver capsules, respectively, for the following carbon and oxygen isotope analyses. However, the cellulose material was insufficient for some long-shoot subsamples either due to little material beforehand or material loss during transfer and homogenization. In some cases, we combined neighboring branch cellulose subsamples into "one branch cellulose subsample" to increase the weight. However, some were still insufficient to suffice for dual isotope analyses. For the 28-cm-long shoot, we prioritized the oxygen isotope analysis. We prepared 23 stem and 68 branch cellulose subsamples for carbon isotope analysis and 27 stem and 80 branch cellulose subsamples for oxygen isotope analysis. For the 7-cm-long shoot, we prioritized the carbon isotope analysis after finding cyclic patterns in  $\delta^{13}\text{C}$  data from the 28-cm-long shoot. We prepared 7 stem and 36 branch cellulose subsamples for carbon isotope analysis and 3 stem and 36 branch cellulose subsamples for oxygen isotope analysis.

#### 2.4. Isotopic measurements

Isotopic analyses were conducted at the Northeast Institute of Geography and Agroecology, Chinese Academy of Sciences, using a state-of-the-art continuous-flow system consisting of an elemental analyzer (FLASH 2000 HT; Thermo Fisher Scientific, USA) and an isotope ratio mass spectrometer (MAT 253; Thermo Fisher Scientific, USA). By

Schematic for subsampling long *Sphagnum* moss shoots  
 (A) stem (17–18 cm section)  
 (B) branch (distance from capitulum: 17.1 cm)  
 (C) clustered branch (distance from capitulum: 17.5 cm)  
 (D) branch (distance from capitulum: 17.9 cm)

convention, isotopic ratios were reported in  $\delta$  notation (per mille) referenced to VPDB (Vienna Pee Dee Belemnite) for  $\delta^{13}\text{C}$  and to VSMOW (Vienna Standard Mean Ocean Water) for  $\delta^{18}\text{O}$ . Several reference materials were routinely measured to ensure data precision and accuracy, including benzoic acid IAEA-601 ( $\delta^{13}\text{C} = -28.81 \pm 0.04 \text{ ‰}$ ;  $\delta^{18}\text{O} = 23.14 \text{ ‰} \pm 0.19 \text{ ‰}$ ), wood powder USGS54 ( $\delta^{13}\text{C} = -24.43 \pm 0.02 \text{ ‰}$ ;  $\delta^{18}\text{O} = 17.79 \pm 0.15 \text{ ‰}$ ) or USGS56 ( $\delta^{13}\text{C} = -24.34 \pm 0.01 \text{ ‰}$ ;  $\delta^{18}\text{O} = 27.23 \pm 0.03 \text{ ‰}$ ), and Elemental Microanalysis reference EMA P2 ( $\delta^{13}\text{C} = -28.19 \pm 0.14 \text{ ‰}$ ;  $\delta^{18}\text{O} = 26.88 \pm 1.88 \text{ ‰}$ ). The analytical precision ( $1\sigma$ ) is better than 0.15 ‰ for  $\delta^{13}\text{C}$  and 0.2 ‰ for  $\delta^{18}\text{O}$ , based on the long-term performance of the instrument (Xia et al., 2024), but we estimate that the precision of  $\delta^{18}\text{O}$  data for some low-weight (0.1–0.15 mg) samples of shoot-dissected stems and branches to be worse at about 0.6 ‰.

A fully detailed description of isotopic measurements, including instrumental setting and procedure, isotope data processing and calibration, as well as uncertainty assessment, is provided in Text S2.

#### 2.5. Field monitoring and weather station data

We set up a monitoring station in the northern open area of Hani peatland to collect local environmental data. It has a sensor measuring air temperature and relative humidity (S-THC-M002; Onset Computer Corp., USA), a rain gauge (S-RGB-M002; Onset Computer Corp., USA), a water table logger (Odyssey; Dataflow Systems, New Zealand) inserted beneath a *Sphagnum*-dominated hummock, and a sonic ranging snow depth sensor (SR50A, Campbell Scientific, Inc., USA). However, these site-specific data did not completely cover the time period of interest, contained some gaps, and had technical limitations. For example, the rain gauge did not measure snow precipitation in winter. The water table logger was removed from the field during the freezing winter. Therefore, we analyzed these site-specific data to validate our subsequent use of government-based, continuous, and quality-controlled weather station data from Jingyu station (30 km northeast of Hani peatland) that were used in temporal matching analysis for long-shoot samples. These two locations are not too close but within the same basin and lack major topographic barriers.

### 3. Results

#### 3.1. Isotopic variations across local microtopographic transects

At the hummock-hollow transect H1, *Sphagnum* moisture content increases steadily from hummock top to hollow, ranging from <900 % to >3000 % (Fig. 3a). The sample farthest from the hummock top, representing the wettest end of the transect, was collected from a standing-water habitat and has the highest moisture content (Figs. 1c and 3a).

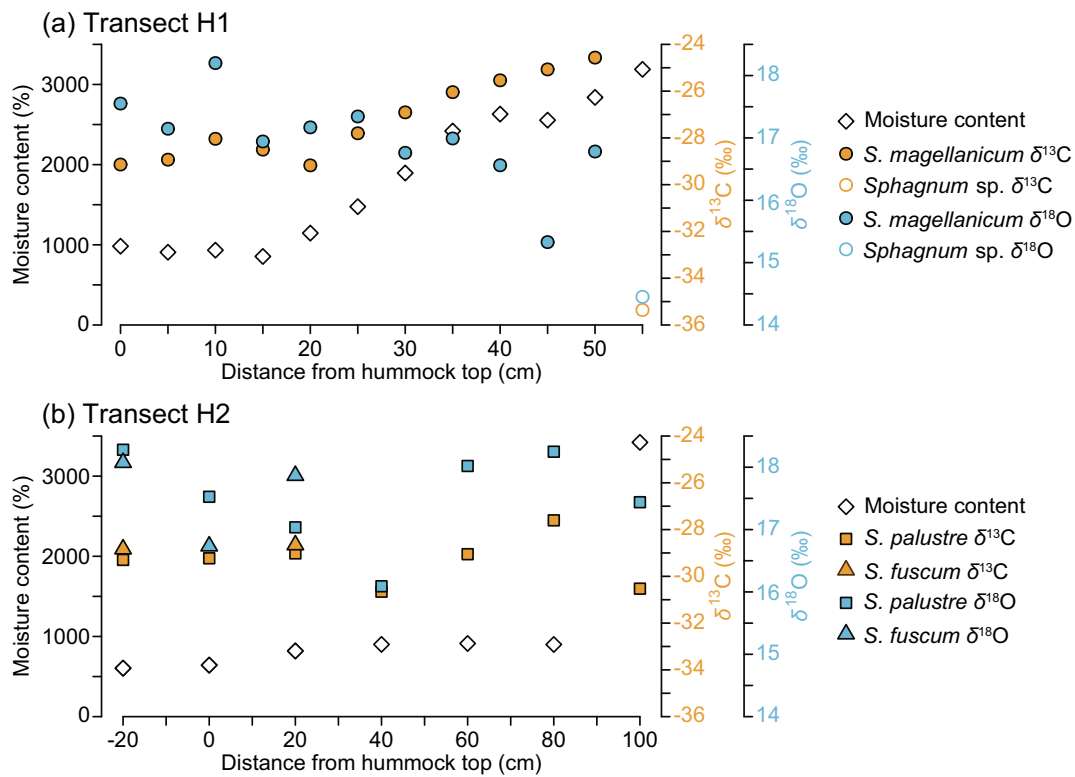


**Fig. 3.** Variations in moisture content (water-to-dry mass ratio; open diamond) and *Sphagnum* cellulose  $\delta^{13}\text{C}$  (orange symbols) and  $\delta^{18}\text{O}$  (blue symbols) across microtopographic transects (a) H1 and (b) H2. Different symbols denote species information. The distance of “-20 cm” for H2 means that the transect extends to the other side of the hummock. (For interpretation of the references to colour in this figure legend, the reader is referred to the web version of this article.)

The exact species could not be confidently identified but likely belongs to subgenus *Cuspidata*. Measured cellulose  $\delta^{13}\text{C}$  values of *S. magellanicum* increase from  $-29.2\text{ ‰}$  to  $-24.6\text{ ‰}$  from hummock top to hollow along the transect, closely following the increasing moisture content, but the  $\delta^{13}\text{C}$  value of *Sphagnum* sp. from the standing-water habitat is extremely low at  $-35.4\text{ ‰}$  (Fig. 3a). Measured cellulose  $\delta^{18}\text{O}$  values generally show a decreasing trend across the same transect, ranging from  $14.5\text{ ‰}$  to  $18.4\text{ ‰}$  (Fig. 3a).

At the hummock-hollow transect H2, *Sphagnum* moisture content varies little, specifically between about 600 % and 900 %, except for the wettest one also collected from a standing-water habitat, with moisture content reaching about 3400 % (Fig. 3b). We have cellulose  $\delta^{13}\text{C}$  and  $\delta^{18}\text{O}$  data for both *S. palustre* and *S. fuscum*, which typically inhabit dry hummocks or lawns (Rydin and Jeglum, 2013), in the three samples closest to the hummock top, and only for *S. palustre* in other samples. Overall, measured cellulose  $\delta^{13}\text{C}$  and  $\delta^{18}\text{O}$  values do not show clear trends across the transect, with narrower ranges from  $-30.7\text{ ‰}$  to  $-27.6\text{ ‰}$  and from  $16.0\text{ ‰}$  to  $18.3\text{ ‰}$ , respectively (Fig. 3b).

Scatter plots clearly show the positive correlation between cellulose  $\delta^{13}\text{C}$  and moisture content and the negative correlation between cellulose  $\delta^{18}\text{O}$  and moisture content (Fig. 4a and b). Two samples collected from standing-water habitats were not shown and will be discussed later. Statistical analysis indicates that these correlations are both significant within the H1 dataset ( $r = 0.96, p < 0.001$ ;  $r = -0.66, p < 0.05$ ), which is derived from the single species *S. magellanicum* across a large and gradual moisture content gradient (Fig. 4a and b). Due to the same dependence of cellulose  $\delta^{13}\text{C}$  and  $\delta^{18}\text{O}$  on *Sphagnum* moisture content, there is also a statistically significant correlation between  $\delta^{13}\text{C}$  and  $\delta^{18}\text{O}$  ( $r = -0.64, p < 0.05$ ; Fig. 4c). The effects of *Sphagnum* moisture content on cellulose  $\delta^{13}\text{C}$  and  $\delta^{18}\text{O}$  are unclear within the H2 dataset largely because of the narrow moisture content gradient itself, but these isotope data do not deviate from the regression lines established from the H1 dataset (Fig. 4).

### 3.2. Isotopic variations of long *Sphagnum* moss shoots

The isotopic signatures of stems and branches along the 28-cm-long shoot of *S. magellanicum* collected from the hummock edge show striking cyclic patterns, where at least four peaks (maxima) and four troughs (minima) can be identified (Fig. 5a and b). Measured stem cellulose  $\delta^{13}\text{C}$  values range from  $-31.6\text{ ‰}$  to  $-27.7\text{ ‰}$ , while branch cellulose  $\delta^{13}\text{C}$  values are relatively higher and vary within a smaller range, from  $-28.1\text{ ‰}$  to  $-25.0\text{ ‰}$  (Fig. 5a). There are significant differences between stem  $\delta^{13}\text{C}$  and branch  $\delta^{13}\text{C}$  data ( $p < 0.001$ , Student's *t*-test). Measured stem and branch cellulose  $\delta^{18}\text{O}$  values range from  $14.8\text{ ‰}$  to  $20.5\text{ ‰}$  and from  $13.4\text{ ‰}$  to  $20.3\text{ ‰}$ , respectively (Fig. 5b), and do not show significant differences in absolute values ( $p = 0.84$ ). For the 7-cm-long shoot of *S. magellanicum* collected from the hummock top, cyclic patterns are far less apparent in cellulose  $\delta^{13}\text{C}$  data, with lower values ranging from  $-30.5\text{ ‰}$  to  $-28.4\text{ ‰}$  for stems and significantly higher values from  $-29.3\text{ ‰}$  to  $-26.5\text{ ‰}$  for branches ( $p < 0.001$ ; Fig. 5c). However, three peaks and two troughs can be clearly identified in branch cellulose  $\delta^{18}\text{O}$  data, which range from  $12.7\text{ ‰}$  to  $19.4\text{ ‰}$  (Fig. 5d). There are only three data points for stem cellulose  $\delta^{18}\text{O}$ , which range from  $14.1\text{ ‰}$  to  $16.7\text{ ‰}$  and have no significant differences from branch cellulose  $\delta^{18}\text{O}$  data ( $p = 0.25$ ; Fig. 5d).

By visually comparing isotopic variations between stems and branches along the shoots, it appears that both  $\delta^{13}\text{C}$  and  $\delta^{18}\text{O}$  shifts always occur at slightly downward positions (farther away from the capitula) in stems than branches (Fig. 5). These position offsets are expected, as branches grow most of their biomass when they are in capitula before being distributed to stems and are older than the stem they attach to (Clymo, 1970; Aldous, 2002; Loader et al., 2007; Yasuda et al., 2015), as shown in a schematic diagram of Fig. 6c. Shifting branch data further away from the capitula to align with stem data would greatly increase the correlation coefficient between stem  $\delta^{13}\text{C}$  and branch  $\delta^{13}\text{C}$  or between stem  $\delta^{18}\text{O}$  and branch  $\delta^{18}\text{O}$ . Their maximum

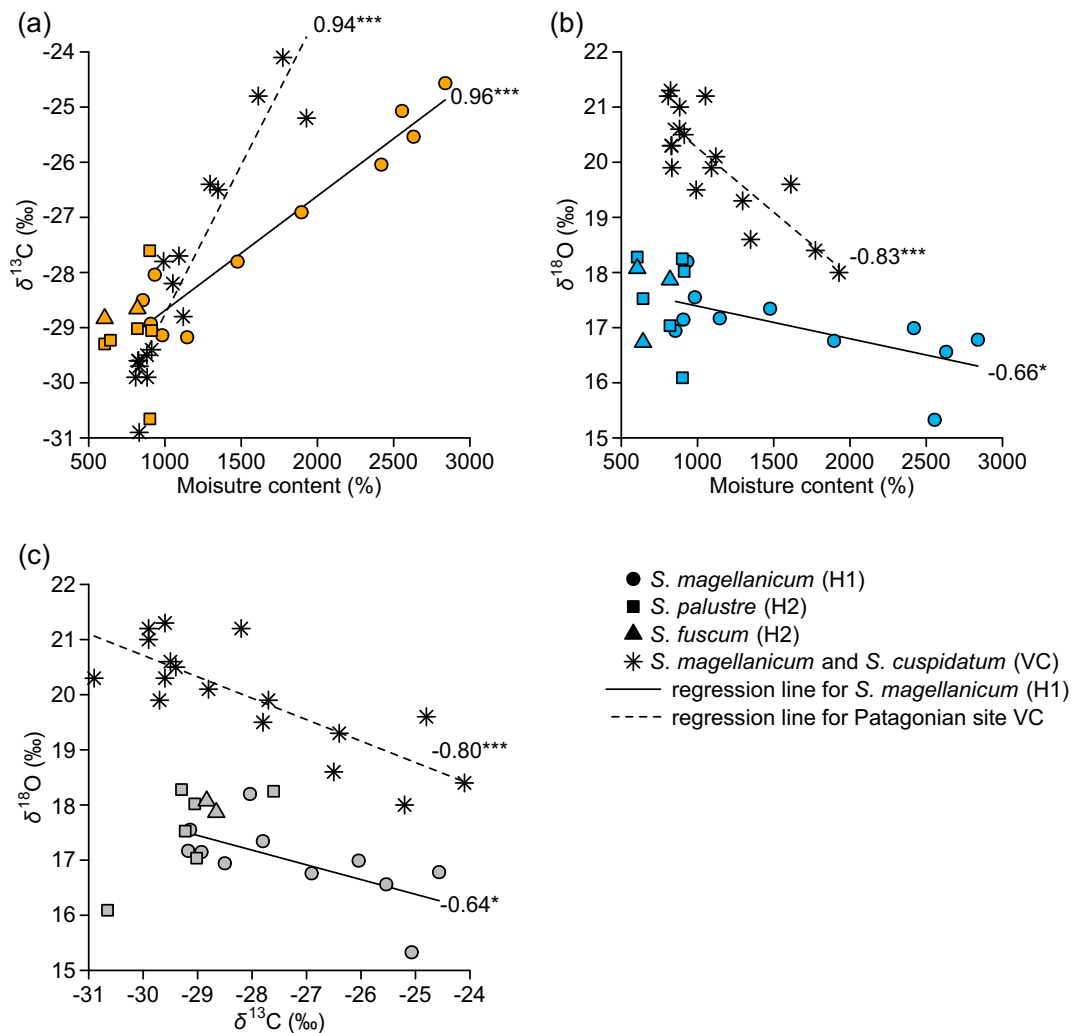


**Fig. 4.** Scatter plots showing the relationships between (a) *Sphagnum* cellulose  $\delta^{13}\text{C}$  and moisture content (water-to-dry mass ratio), (b) *Sphagnum* cellulose  $\delta^{18}\text{O}$  and moisture content, and (c) *Sphagnum* cellulose  $\delta^{18}\text{O}$  and  $\delta^{13}\text{C}$ . Two samples collected from standing-water habitats were excluded. Different symbols distinguish the species and transect. Asterisks represent published data collected from a microtopographic transect from the site Valle de Consejo (VC) in southern Patagonia (Xia et al., 2020). Solid and dashed lines represent regression lines for *S. magellanicum* datasets from transect H1 of this study and the transect from the Patagonian site VC, respectively. Their correlation coefficients are shown beside (\* $p < 0.05$ , \*\*\* $p < 0.001$ ).

correlation coefficients are achieved when shifting branch data by about 1.5 cm for the 28-cm-long shoot and about 0.5 cm for the 7-cm-long shoot, respectively (Fig. 6a and b). After introducing this distance offset, there is a particularly remarkable overlap in terms of the phase of cycles and amplitude of corresponding peaks and troughs between stems and branches for both  $\delta^{13}\text{C}$  and  $\delta^{18}\text{O}$  data of the 28-cm-long shoot (Fig. 7); so does the 7-cm-long shoot (not shown). There is a slightly different trough pattern between the “mirrored check mark” shape of stem  $\delta^{13}\text{C}$  and the “V” shape of branch  $\delta^{13}\text{C}$  in the 28-cm-long shoot (Fig. 7a), but we show in Appendix A that this can be explained by different growing processes of the two tissues and a wider time window of  $\delta^{13}\text{C}$  signatures. The systematic differences between stem  $\delta^{13}\text{C}$  and branch  $\delta^{13}\text{C}$  are also expected, as already observed in several previous studies and attributed to biochemical factors (Loader et al., 2007; Yasuda et al., 2015; Xia et al., 2025).

Overall, our analysis uncovers cyclic isotopic variations of considerable magnitudes in dissected growth increments of long *Sphagnum* moss shoots. By accounting for position offsets, stem and branch increments from the same shoot exhibit similar temporal changes in isotopic signatures. As discussed later, these peak-and-trough patterns in isotopic signatures can be interpreted as seasonal cycles and analyzed as time series against instrumental data back to the last several years at

sub-annual resolution. The peaks and troughs of  $\delta^{13}\text{C}$  do not coincide with the peaks and troughs of  $\delta^{18}\text{O}$  in either the stem or branch samples for both shoots, reflecting their different controlling factors and resulting in no statistically significant correlation between the  $\delta^{18}\text{O}$  and  $\delta^{13}\text{C}$  data (Fig. 8). The cyclic isotopic variations differ between the two different shoots (Fig. 5). The  $\delta^{18}\text{O}$  peak closest to the capitulum is highest for the 7-cm-long shoot but not so for the 28-cm-long shoot (Fig. 5b and d). The highly resolved branch  $\delta^{13}\text{C}$  data of the 7-cm-long shoot do not show strong cyclic patterns as found in the  $\delta^{13}\text{C}$  data for the 28-cm-long shoot (Fig. 5a and c).

### 3.3. Weather station-based climate records and local validations

Weather station data from Jingyu station show large inter-annual variability in summer monsoon precipitation during the preceding five years (Fig. 9a). The May–September total precipitation amount is higher in wet years 2022, 2020, and 2018, and lower in dry years 2021 and 2019 (Fig. 9a). The anomalies from 2022 back to 2018 are +51 %, -11 %, +33 %, -14 %, and +19 %, respectively, compared to the long-term average (624 mm, during the period 1981–2010). For the winter half-year, we use the November–April total precipitation amount to estimate winter snow accumulation that may control the moisture

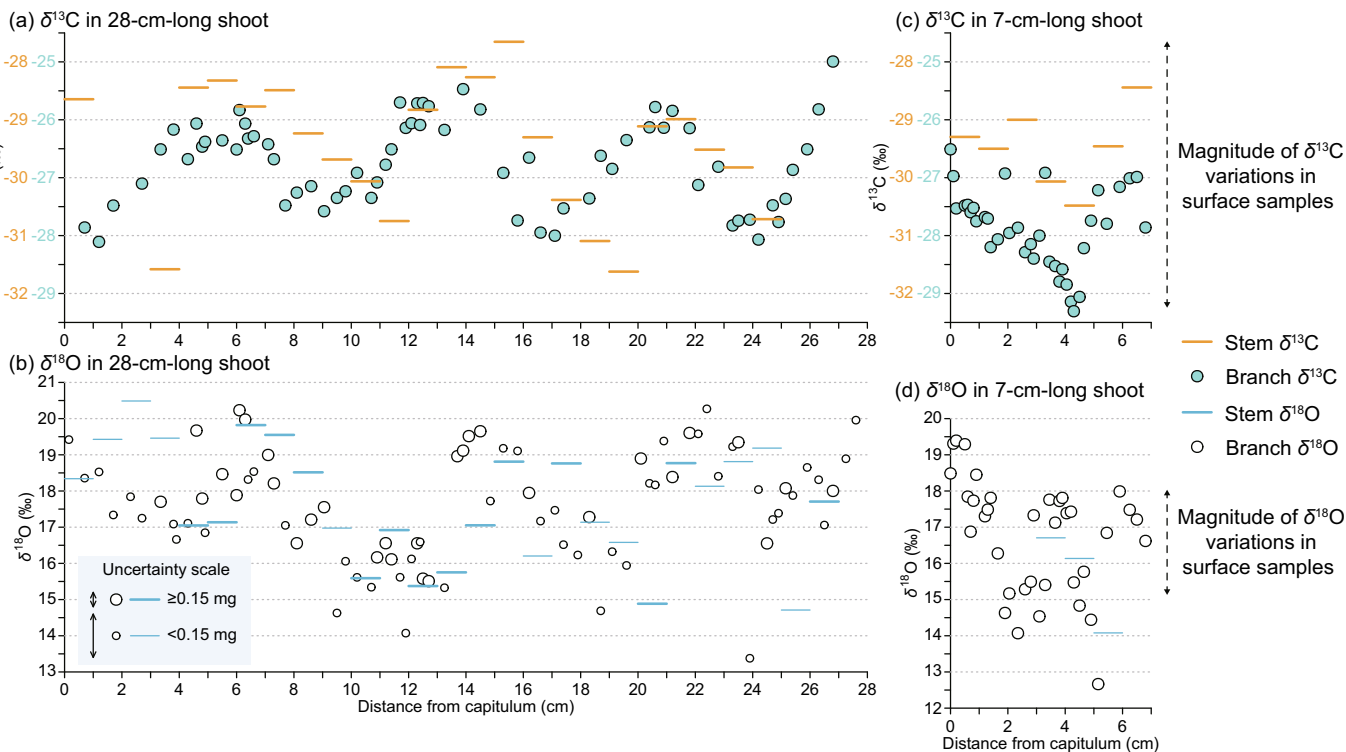


**Fig. 5.** Isotopic variations of long *Sphagnum* moss shoots plotted against the distance from the capitula. The left side is the results of (a)  $\delta^{13}\text{C}$  and (b)  $\delta^{18}\text{O}$  derived from the 28-cm-long shoot of *S. magellanicum* collected from the hummock edge. The right side is the results of (c)  $\delta^{13}\text{C}$  and (d)  $\delta^{18}\text{O}$  derived from the 7-cm-long shoot of *S. magellanicum* collected from the hummock top. Stem data are plotted as 1-cm horizontals, and branch data are plotted as dots. For  $\delta^{18}\text{O}$  data, the size of the dots and the thickness of the horizontals are based on the weight of measured cellulose, where low-weight samples (<0.15 mg) should be interpreted with larger analytical uncertainties of 0.6 ‰ compared to regular-weight samples of 0.2 ‰ (Section 2.4). On the rightest side, dashed arrows provide a reference for the magnitudes of  $\delta^{13}\text{C}$  and  $\delta^{18}\text{O}$  variations (4.6 ‰ and 2.9 ‰, respectively) in surface *S. magellanicum* samples (i.e., Fig. 3a).

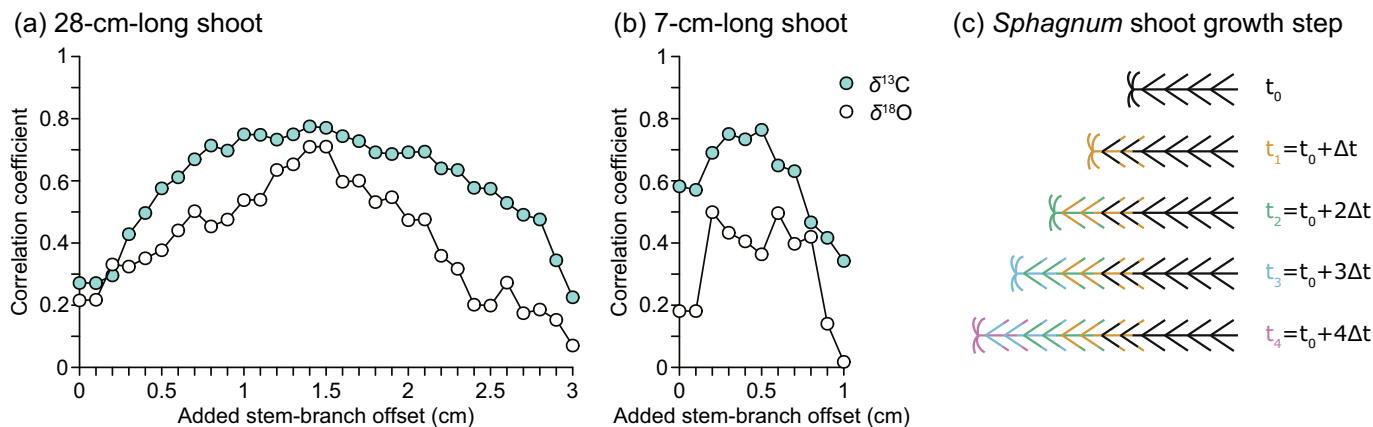


**Fig. 6.** The correlation coefficient of isotope data between stems and branches after adding a certain distance offset to move branch data to downward (farther away from capitula) positions for the (a) 28-cm-long shoot and (b) 7-cm-long shoot. Cyan and open dots refer to the  $\delta^{13}\text{C}$  and  $\delta^{18}\text{O}$  data, respectively. (c) Schematic diagram of *Sphagnum* shoot growth over hypothetical timesteps. Tissues synthesized during different timesteps are marked in different colors (modified from Aldous, 2002). (For interpretation of the references to colour in this figure legend, the reader is referred to the web version of this article.)

availability in the coming start of the new growing season after snowmelt (Fig. 9a). The anomalies are +33 %, -5 %, +29 %, and -37 % in years 2021–2022, 2020–2021, 2019–2020, and 2018–2019, respectively, compared to the same long-term average (117 mm). Relative humidity (RH) shows large seasonality and is lowest in April when the temperature is just above freezing and the summer monsoon has not yet arrived, a period known as the “dry and windy spring” in Northeast China (Fig. 8b; Zhang and Hu, 2018). It has subtle inter-annual variability except for the November–April RH of the 2018–2019 dry winter (60 %), which is much lower than other years (67–70 %), and the low

RH continues into May 2019 (Fig. 9b). For temperature data, the calculated May–September temperature varies very little, only between 17.5 °C and 17.7 °C during the last five years except in 2022 (17.0 °C) when we collected the samples (Fig. 9c). However, the calculated February–April temperature, which we consider as a simple metric affecting the onset of the growing season and the strength of spring production, is -0.4 °C in early 2021 (warm late winter–early spring), higher than other years in which it varies between -2.3 °C and -1.7 °C (Fig. 9c).

Monitoring station data from Hani peatland support the use of continuous and robust climate data from Jingyu station to represent

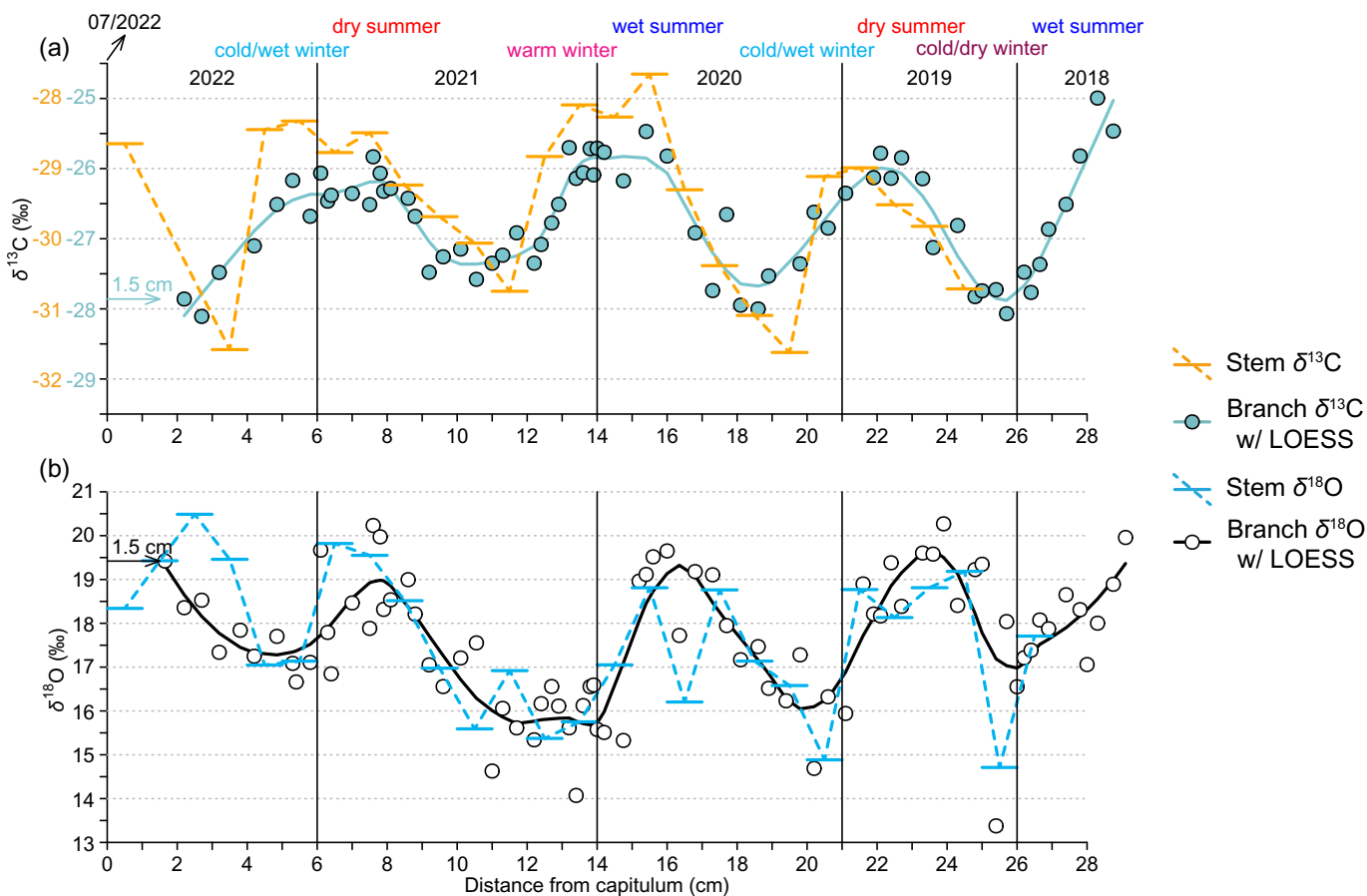


**Fig. 7.** Isotopic variations of the 28-cm-long *Sphagnum* moss shoot plotted against the distance from the capitulum, as already shown in Fig. 5a and b, but branch data are shifted “downward” by 1.5 cm to account for the position offset and “synchronize” stem and branch growth. Stem data are further connected by straight dashed lines, and branch data are fitted with a LOESS (locally estimated scatterplot smoothing) curve ( $\alpha = 0.2$ ). Vertical lines indicate the positions that we infer possible cycles of growing seasons based on cellulose  $\delta^{18}\text{O}$  data. The top panel summarizes climate information derived from instrumental data for the respective years (see Section 4.2 for further details). The newest stem growth below the capitulum should be shortly before the time of sample collection (July 2022).

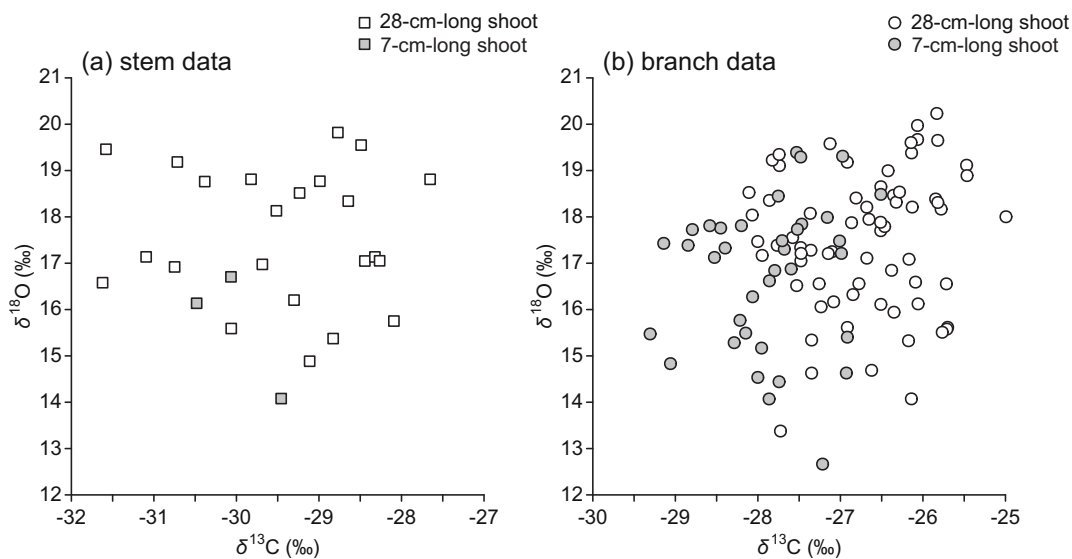


**Fig. 8.** Scatter plots showing the relationships between *Sphagnum* cellulose  $\delta^{18}\text{O}$  and  $\delta^{13}\text{C}$  in (a) stems and (b) branches in two analyzed long *Sphagnum* moss shoots.

climate conditions at our site on seasonal and inter-annual timescales. These two locations are remarkably similar in seasonal and inter-annual changes in climate conditions with correlation coefficients of 0.99, 0.95, and 0.97 for monthly temperature, precipitation, and RH, respectively

(Fig. S1). Data from other weather stations further indicate that the above described climate anomalies observed at Jingyu station in specific years are robust regional-scale signals (Figs. S2–S5). Available water table measurements at Hani peatland show a sensitive response of local

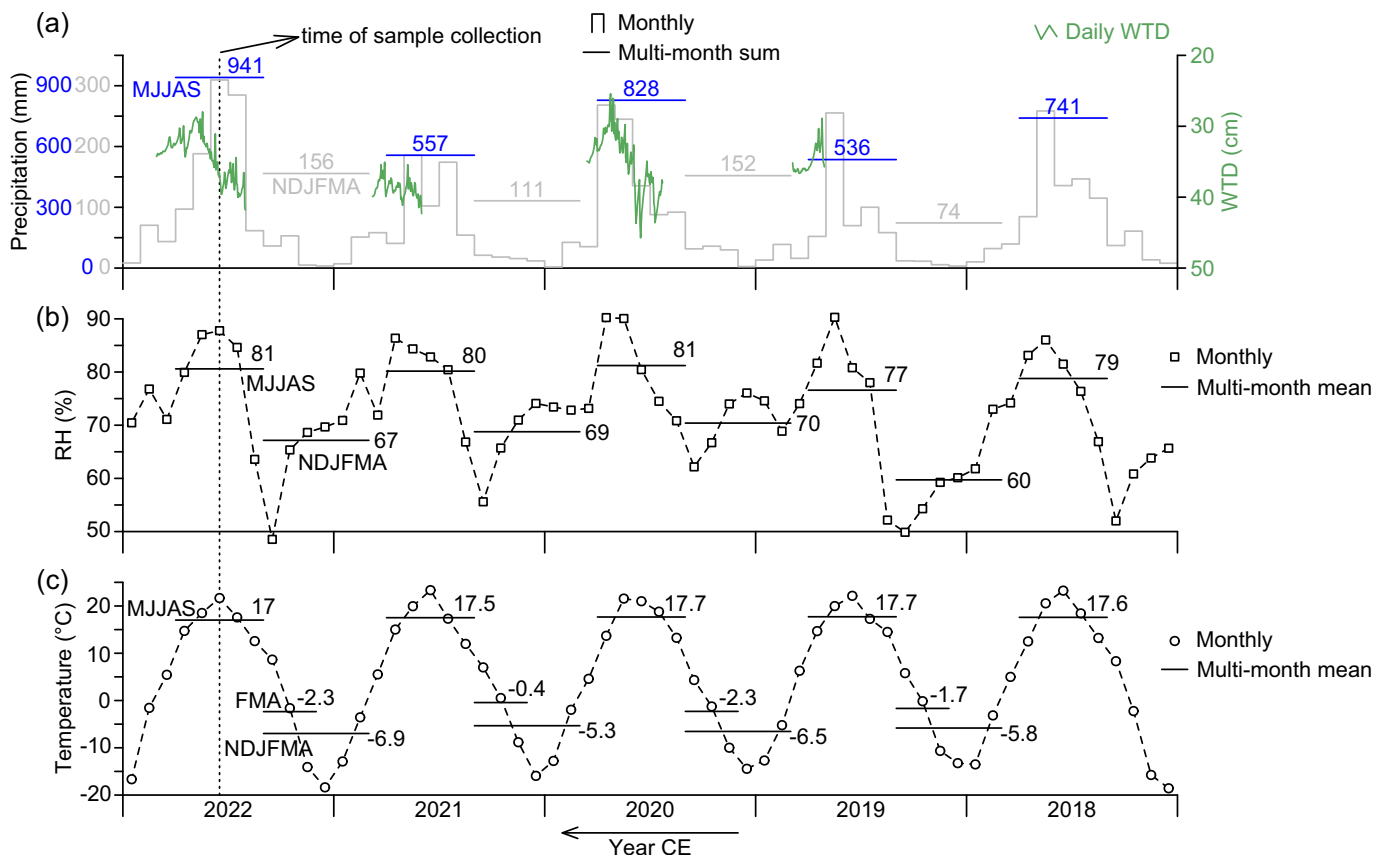


**Fig. 9.** Monthly climate data from Jingyu station from 2018 to 2022. (a) Monthly precipitation (gray line), total precipitation of the summer monsoon season (May–September, MJJAS; blue lines and labels), and total precipitation of the winter half-year (November–April, NDJFMA; gray lines and labels). Also shown are available daily water table depth (WTD; green line) data at Hani peatland. (b) Monthly relative humidity (RH) and average RH of the summer monsoon season (MJJAS) and the winter half-year (NDJFMA). (c) Monthly temperature and average temperature of the summer monsoon season (MJJAS), the winter half-year (NDJFMA), and the late winter–early spring period (February–April, FMA). (For interpretation of the references to colour in this figure legend, the reader is referred to the web version of this article.)

moisture conditions to precipitation variability (Fig. 9a). The water table depth (WTD) is higher (drier condition) in early summer and lowest (wettest condition) in late summer (late August–early September) in response to the continuous input of summer monsoon precipitation into the site (Fig. 9a). The WTD is indeed lower in wet years 2022 and 2020 and higher in dry years 2021 and 2019 (Figs. 9a and S6). Finally, available snow depth measurements support that snow cover is present at our site during the winter half-year (from November to April) when the local daily temperature is below freezing (Fig. S7).

#### 4. Discussion

##### 4.1. Confirmation of water film and evaporative enrichment effects from space-for-time substitution

The isotopic analyses of surface *Sphagnum* samples repeat what was shown in our previous study in southern Patagonia, which also reported similar patterns for *S. magellanicum* across a well-characterized microtopographic transect (Fig. 4; Xia et al., 2020). These results are in agreement with the water film effect on  $\delta^{13}\text{C}$ , the evaporative enrichment effect on  $\delta^{18}\text{O}$ , as well as their potential coupling (Xia et al., 2020). The difference lies in the relatively shallower slope between  $\delta^{13}\text{C}$  and moisture content or between  $\delta^{18}\text{O}$  and moisture content in this new dataset, whereas the slopes between  $\delta^{13}\text{C}$  and  $\delta^{18}\text{O}$  remain similar between the two studies (Fig. 4).

The two data points related to standing-water habitats differ from the general patterns and warrant proper interpretations (Fig. 3). For the *Sphagnum* sp. sample from transect H1 (Fig. 3a), its very low  $\delta^{13}\text{C}$  value

is not a new finding and was previously reported for hollow-inhabiting species (Proctor et al., 1992; Price et al., 1997; Markel et al., 2010; Zibulski et al., 2017). These studies all hypothesize that it might be related to physiological adaptation allowing them to use non-atmospheric carbon, including methane-derived  $\text{CO}_2$ , which is known to be very depleted in  $^{13}\text{C}$  (Raghoebarsing et al., 2005). Its very low  $\delta^{18}\text{O}$  value might be partly related to the preferential use of standing water connected to the peatland drainage network of surface inflows (Zanazzi and Mora, 2005), in contrast to nutrient-poor *S. magellanicum* on hummocks that tend to rely on precipitation for growth. This is supported by snapshot isotopic measurements of standing water collected close to transect H1 during fieldwork, showing relatively lower values ( $-11.7\text{\textperthousand}$ ; Fig. S8) than modeled climatological mean precipitation ( $-8\text{\textperthousand}$ ) in May–July (see following Fig. 10a) preceding the time of sampling. For the *S. palustre* sample from transect H2, its  $\delta^{13}\text{C}$  and  $\delta^{18}\text{O}$  values are similar to other samples from the same transect (Fig. 3b), suggesting that the standing-water condition and high moisture content are likely ephemeral.

The above space-for-time substitution method utilizing the natural environmental gradients within peatlands for calibrating isotopic proxies, however, does not address the magnitude and pattern of their variability under temporally changing environmental conditions.

##### 4.2. Inferred sub-annual isotopic courses for long *Sphagnum* moss shoots

In this section, we aim to justify how to interpret cyclic isotopic variations along the *Sphagnum* moss shoots as isotopic time series. We focus on the 28-cm-long shoot due to its rapid length increment, high-

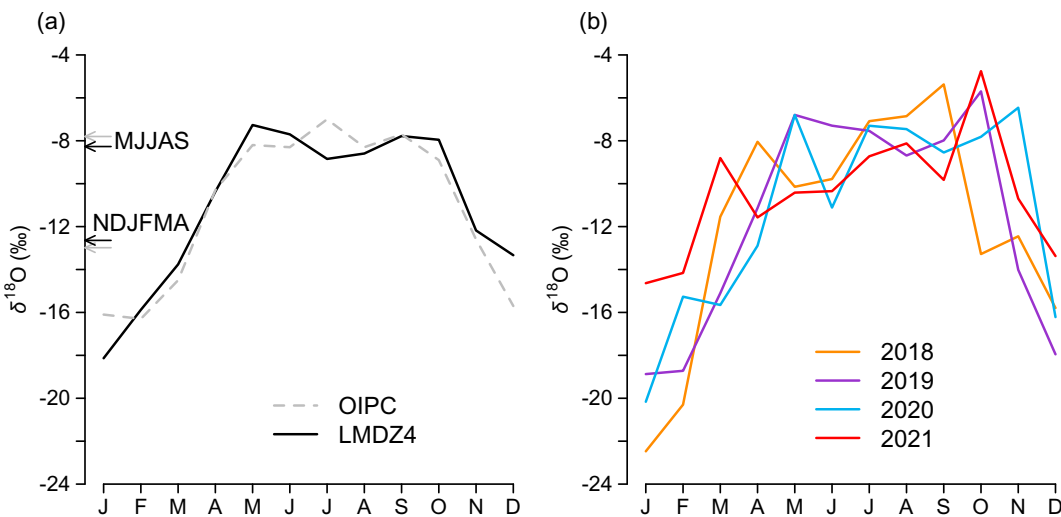


**Fig. 10.** (a) Twelve-monthly climatological mean precipitation  $\delta^{18}\text{O}$  at Hani peatland derived from the observation-based geostatistical model OIPC (gray dashed line; Bowen et al., 2005) and the isotope-enabled general circulation model LMDZ4 (black line; Risi et al., 2012). See Appendix B for details. Their amount-weighted means during the summer monsoon season (May–September, MJJAS) and the winter half-year (November–April, NDJFMA) are marked with colored arrow symbols on the left. (b) Monthly precipitation  $\delta^{18}\text{O}$  at Hani peatland in individual years of 2018–2021 from the LMDZ4 model (output for 2022 is not available).

resolution of measured data, and multiple well-resolved data.

Due to the persistent cyclic fluctuations observed in both  $\delta^{13}\text{C}$  and  $\delta^{18}\text{O}$  data from the 28-cm-long shoot (Fig. 7), alongside the large climate seasonality at our site (Fig. 9), it is reasonable to associate these cycles with yearly patterns (Yasuda et al., 2015; Xia et al., 2020), as alternative scenarios lack evident mechanisms. Based on the number of cycles, we can estimate the averaged growth rate for the 28-cm-long hummock-edge shoot as about 7 cm/year. From the clear cycles in  $\delta^{18}\text{O}$  data from the 7-cm-long hummock-top shoot, we can estimate the averaged growth rate to be about 3 cm/yr. A previous study at the same site, using a wire-based approach, measured the annual growth rate of the same species from hummock top habitats to be 0–4.6 cm/yr (Bengtsson et al., 2021), and our recent wire-based measurements in 2024 found that the growth rates from hummock edge habitats range from 1.3 to 6.3 cm/yr from mid-May to mid-October (Fig. S9). Thus, the inferred growth rate for the 7-cm-long shoot falls within the common range but for the 28-cm-long shoot appears to be at the highest end of the variation. The latter is still reasonable and expected, as we intentionally analyzed the longest and presumably fastest-growing shoot, a methodological bias previously recognized by Yasuda et al. (2015).

We next need a criterion to divide the seasonal cycles in the isotopic time series. This process is going to be subjective, as annual *Sphagnum* length increments are not constant (Luken, 1985; Moore, 1989; Koronatova et al., 2022). We suggest that cyclic fluctuations of cellulose  $\delta^{18}\text{O}$  along the shoot primarily reflect seasonal changes of precipitation  $\delta^{18}\text{O}$ , and that abrupt decreases of cellulose  $\delta^{18}\text{O}$  are potential markers for the start of a new year's growth based on several considerations:

- (1) There is a strong seasonal cycle of precipitation  $\delta^{18}\text{O}$  at our site with a magnitude of 8 ‰ in monthly mean values or a 4 ‰ difference between the summer monsoon season (May–September, MJJAS) and the winter half-year (November–April, NDJFMA) (Fig. 10a and Appendix B).
- (2) Although the long, extremely cold winter at our site does not allow plant production, *Sphagnum* mosses are opportunistic plants and can grow during the earliest growing season (Asada et al., 2003; Genet et al., 2013; Küttim et al., 2020) as long as the daytime temperature reaches 0 °C even before the complete disappearance of snow cover (Moore et al., 2006; Loisel et al., 2012). This earliest growth coincides with the timing of spring snowmelt released from the local snowpack and is, therefore,

expected to capture the low  $\delta^{18}\text{O}$  signal in accumulated winter precipitation (Kaislahti Tillman et al., 2013; Xia et al., 2025).

- (3) Both empirical data and process-based models have shown that *Sphagnum* moss cellulose  $\delta^{18}\text{O}$  is highly sensitive to variability in source water  $\delta^{18}\text{O}$  (Daley et al., 2010; Granath et al., 2018; Royles et al., 2022). The magnitude of difference between  $\delta^{18}\text{O}$  peaks (19–20 ‰) and troughs (15–17 ‰) for the 28-cm-long shoot is close to that in modeled climatological mean precipitation between MJJAS (−8 ‰) and NDJFMA (−12 ‰) periods in this region (Figs. 7b and 10a). The corresponding offsets between cellulose  $\delta^{18}\text{O}$  peaks/troughs and mean MJJAS/NDJFMA precipitation  $\delta^{18}\text{O}$  are also similar to the biochemical fractionation factor of 27 ‰ by <2 ‰ (Sternberg et al., 1986). These provide further support for the close link between precipitation  $\delta^{18}\text{O}$  and cellulose  $\delta^{18}\text{O}$ . Notably, *S. magellanicum* favors nutrient-poor habitats and does not occur with standing water at our site.
- (4) Precipitation  $\delta^{18}\text{O}$  remains high from summer until October—the last above-freezing month of the year (Fig. 10). Thus, any plant production at the end of the growing season plays a minor role in explaining the abrupt shifts toward lower cellulose  $\delta^{18}\text{O}$  observed in our data.
- (5) The evaporative enrichment effect may modulate cellulose  $\delta^{18}\text{O}$  values but it should be minimized for the 28-cm-long shoot collected from wet hummock edge habitats (Section 4.1). Additionally, our site, being in a humid region, is not prone to strong evaporative enrichment as shown in our snapshot isotopic measurements of peatland surface water (Fig. S8).

Using the  $\delta^{18}\text{O}$  marker, we can tentatively anchor the seasonal cycles for the 28-cm-long shoot as follows: years 2021, 2020, and 2019 correspond to stem sections at 6–14 cm, 14–21 cm, and 21–26 cm distances from the capitulum, respectively, while years 2022 and 2018 are incompletely documented in stem sections of 0–6 cm and 26–28 cm, respectively (Fig. 7). We can further infer that the sub-annual course of  $\delta^{13}\text{C}$  data is characterized by a peak-trough-peak sequence, except for a possible abnormal year of 2019 (Fig. 7a). As an additional constraint, the timing of  $\delta^{13}\text{C}$  troughs can be anchored to earlier than mid-summer, most likely in spring, because the newest stem just below the capitulum—which is no later than early July of 2022—has reached the peak phase of  $\delta^{13}\text{C}$  (Fig. 7a). Based on the water film effect revealed in surface *Sphagnum* mosses, we can interpret the sub-annual course of  $\delta^{13}\text{C}$  data with temporal matching as a wet-dry-wet transition, consistent with the

expected seasonal sequence of snowmelt, the “dry and windy spring” after snowmelt but before monsoon intrusion, and full summer monsoon state at our site (Fig. 9). For  $\delta^{18}\text{O}$  data, the values increase over the course of the seasonal cycle, reflecting the transition from the use of spring snowmelt to summer precipitation, in part because we have already anchored the start of a new year at low  $\delta^{18}\text{O}$  values (Fig. 7b).

By focusing on the well-characterized 28-cm-long shoot, the above discussion suggests that cyclic isotopic variations along the *Sphagnum* moss shoots can be reasonably interpreted as seasonal cycles back in time in response to changing environmental conditions, with peaks and troughs corresponding to different timings of a year.

#### 4.3. Are changing levels and durations of isotopic peaks and troughs related to inter-annual climate variability?

The highly resolved  $\delta^{13}\text{C}$  and  $\delta^{18}\text{O}$  data from the 28-cm-long shoot also show that the levels or durations of isotopic peaks and troughs vary among cycles (Fig. 7). Based on instrumental records validated by local environmental data (Section 3.3), it is definitely interesting to further explore whether such distinguishable cycle-to-cycle differences reflect the temporal response of isotopic signatures to inter-annual climate variability.

We find evidence that the peak  $\delta^{13}\text{C}$  values in each cycle, which should be late-summer signals representing the wettest time of the year (Fig. 9a), are likely linked to the amount of summer monsoon precipitation in that year. Specifically, these  $\delta^{13}\text{C}$  peaks are higher in the wet summers of 2020 and 2018, and lower in the dry summers of 2021 and 2019 (Fig. 7a), consistent with the previously recognized water film effect. Since  $\delta^{13}\text{C}$  troughs are thought to be post-snowmelt spring signals representing the driest time of the year, we expect a similar water film effect from winter half-year precipitation, which should affect spring moisture availability and thus  $\delta^{13}\text{C}$  values. However, the data indicate the opposite, with lower  $\delta^{13}\text{C}$  trough values after the wet winters of 2021–2022 and 2019–2020, and a higher  $\delta^{13}\text{C}$  trough value after the dry winter of 2020–2021 (Fig. 7a). Instead, we hypothesize that trough  $\delta^{13}\text{C}$  values are likely controlled by the hydrological carry-over effect, becoming higher if the previous summer monsoon season was wetter, and vice versa (Fig. 7a). An exception is the lower  $\delta^{13}\text{C}$  trough value of 2019 coming after the higher  $\delta^{13}\text{C}$  peak value of 2018. This possibly can be linked to the abnormally dry winter half-year of 2018–2019 (Figs. 7a, 9a, and b).

For noisier  $\delta^{18}\text{O}$  data, the most notable feature is the long and deep  $\delta^{18}\text{O}$  trough in 2021, which has an unusually warm late winter–early spring period (Figs. 7b and 9c). This pattern is contrary to the prevailing knowledge that precipitation  $\delta^{18}\text{O}$  is positively correlated with temperature in cold regions or seasons shown in observational datasets, Rayleigh distillation theory, and isotope-enabled climate models (Dansgaard, 1964; Jouzel et al., 2000; Bowen, 2008). The general circulation model (GCM) LMDZ4 model successfully simulates higher precipitation  $\delta^{18}\text{O}$  during the first few months of year 2021 compared to other years (Fig. 10b). The mechanism for this unexpected pattern is unclear. Nevertheless, we hypothesize that it may occur if *Sphagnum* mosses have an early onset of the growing season and can efficiently utilize the low- $\delta^{18}\text{O}$  spring snowmelt for plant production when the late winter–early spring temperature is high, thereby recording a long duration and a large magnitude of the  $\delta^{18}\text{O}$  trough in growth increments.

This temporal matching analysis is exploratory owing to that the results are from a single shoot and that the other 7-cm-long shoot collected from a contrasting habitat shows different patterns of temporal isotopic variations. We emphasize that the causes of distinguishable changes in such isotopic peaks and troughs warrant further investigation and that the processes and mechanisms driving isotopic responses to temporally varying environmental conditions likely differ across peatland habitats.

#### 4.4. Assessments of long-shoot analysis methodology: Strengths, shortcomings, and limitations

The millimeter-scale sequential analysis of *Sphagnum* growth increments presented in this study firmly demonstrates that multiple seasonally resolved cycles of both  $\delta^{13}\text{C}$  and  $\delta^{18}\text{O}$  signatures can be identified within a single *Sphagnum* moss shoot. Compared to previous studies that repeatedly and destructively sample newest growth parts at different times of the year (Daley et al., 2010; Amesbury et al., 2015a; Amesbury et al., 2015b; Royles et al., 2022), our approach ensures that a continuous, high-resolution isotopic time series can be derived from the same specimen without requiring multiple sampling campaigns. Furthermore, it has the potential to capture the earliest and latest growing-season signals when field conditions prevent access to remote sites for sample collections (Dorrepaal et al., 2004; Küttim et al., 2020). This analytical innovation is important for allowing us to accurately characterize the full range and pattern of temporal variability in isotopic signatures of *Sphagnum* mosses on short timescales, which is previously unrecognized in studies based on the space-for-time substitution (Xia et al., 2025).

Although our long-shoot analysis is highly detailed and high-resolution, an important shortcoming of our approach is that we are unable to build a precise intra-annual chronology along the shoot. Instead, we rely on isotopic time markers to divide seasonal cycles. Therefore, we consider it more realistic to qualitatively explore whether a potential link between distinct isotopic peaks or troughs (in terms of magnitude and duration) and major inter-annual climate anomalies can be found (Fig. 7). At this stage, the development of this approach still benefits from additional analyses of tissue samples collected at different times of the year (with known timing of growth; Daley et al., 2010; Royles et al., 2022) or from field-based growth rate measurements (Clymo, 1970; Norby et al., 2019) to better constrain the chronology of isotopic time series. These supporting data would be crucial for confidently applying this approach to multiple specimens or across larger scales in the future.

There are also limitations in our study that should be recognized. First, the temporal matching analysis is hindered by the lack of replications from multiple specimens. The differing pattern of isotopic variations between two contrasting shoots also means that any link between peak-and-trough patterns and instrumental records does not necessarily apply to all habitats or even other individual moss shoots (Fig. 5). Nevertheless, our study indicates, shown from temporal changes in isotopic signatures between stem and branch increments (Fig. 7), that future studies pursuing temporal calibration may only need to analyze the stem tissues to decrease the analytical cost.

Second, we lack complete sets of local environmental data. Specifically, we did not obtain *Sphagnum* moisture content data to test the temporal persistence of the water film effect as we did for surface *Sphagnum* samples. Fortunately, we have non-continuous WTD data to support the potential link among monsoon precipitation, peatland moisture availability, and *Sphagnum*  $\delta^{13}\text{C}$  signals on seasonal and inter-annual timescales (Figs. 7a and 9a). We also did not have actual site-specific precipitation and *Sphagnum* leaf water  $\delta^{18}\text{O}$  measurements from preceding years to quantitatively interpret  $\delta^{18}\text{O}$  data, aside from model-based precipitation  $\delta^{18}\text{O}$  estimates and some snapshot data from peatland surface water samples (Figs. 10 and S8). From our previous study, we are aware that collecting the exact metabolic leaf water involved in cellulose biosynthesis from *Sphagnum* mosses is technically difficult, with inconsistent results presented in the literature (Amesbury et al., 2015a; Loader et al., 2016; Ooki et al., 2018; Xia et al., 2020). Collecting full sets of relevant environmental data and improving water sample collection techniques should be considered in the future for a quantitative analysis of isotopic signals in growth increments.

Finally, this study alone is not able to fully address the current debate in the literature—namely, the relative importance of temperature and moisture availability on *Sphagnum*  $\delta^{13}\text{C}$  and of precipitation  $\delta^{18}\text{O}$  and

evaporative enrichment on *Sphagnum*  $\delta^{18}\text{O}$  in peat-based paleoenvironmental records (Section 1). In this study, we interpret *Sphagnum*  $\delta^{13}\text{C}$  data in growth increments as reflecting moisture availability based on the water film effect, supported by the hummock-hollow transect dataset (Fig. 4). Downplaying the role of temperature is also justified by the fact that only the large inter-annual variability of precipitation, rather than the very small inter-annual variability in temperature (except for one abnormally warm early growing season in 2021), can account for the clearly variable levels of  $\delta^{13}\text{C}$  peaks and troughs found in the 28-cm-long shoot (Figs. 7a and 9). We also interpret *Sphagnum*  $\delta^{18}\text{O}$  data in growth increments as reflecting the temporal transition from the use of spring snowmelt to summer precipitation and suggest that the evaporative enrichment effect cannot predominate over the source water effect. To separate and quantify these multiple effects, future studies may consider collecting a large dataset of isotopic values and environmental variables for rigorous statistical tests (Granath et al., 2018).

Despite the shortcomings and limitations, our long-shoot analysis still allows us to gain important new insights into *Sphagnum* isotopic proxies, as discussed in the following.

#### 4.5. Implications for *Sphagnum* $\delta^{13}\text{C}$ and $\delta^{18}\text{O}$ paleoenvironmental proxies

The highly variable isotopic signatures in the dissected growth increments of *Sphagnum* mosses are comparable in magnitude to those across hummock-hollow transects for  $\delta^{13}\text{C}$  and twice as large as for  $\delta^{18}\text{O}$  (Fig. 5). This suggests that the popular space-for-time substitution applied in several previous studies does not fully capture the natural variability of isotopic signatures (Ménot and Burns, 2001; Ménot-Combes et al., 2002; Loisel et al., 2009; Loader et al., 2016; Granath et al., 2018; Xia et al., 2020) and may bias proxy interpretations in paleoenvironmental reconstructions.

The cyclicity of  $\delta^{13}\text{C}$  and  $\delta^{18}\text{O}$  data, respectively interpreted as reflecting seasonal shifts in moisture availability and plant source water  $\delta^{18}\text{O}$ , indicates that their millimeter-scale growth increments are capable of documenting gradual but large seasonal changes in local environmental conditions. In traditional peat-based paleoenvironmental reconstructions using isotopic proxies, researchers often subsample a sliced layer of a peat core, from which many stem or leaf macrofossils are collected, extracted for cellulose, homogenized, and measured for isotopic compositions. The obtained data are interpreted as reflecting long-term changes in mean growing-season conditions at a resolution of decades or centuries due to the slow accumulation rates of peat deposits (Daley et al., 2010; Xia et al., 2018; Loisel et al., 2023). Based on the high sensitivity of isotopic signatures in *Sphagnum* mosses to seasonality revealed in this study, we argue that such interpretations are too simplistic and have not considered the season-related factors, processes, and mechanisms that control *Sphagnum*  $\delta^{13}\text{C}$  and  $\delta^{18}\text{O}$  signatures.

First, our study indicates the need to consider whether inferred changes in environmental conditions from isotopic proxies result from the influence of a particular season. For example, shifts to lower “mean-state”  $\delta^{13}\text{C}$  values, generally interpreted as indicating drier conditions, may arise either from a drier wet season (lower  $\delta^{13}\text{C}$  peaks in growth increments), a drier dry season (lower  $\delta^{13}\text{C}$  troughs in growth increments) (Fig. 11). Likewise, shifts to lower “mean-state”  $\delta^{18}\text{O}$  values may also be attributed to season-specific lower precipitation  $\delta^{18}\text{O}$ . More importantly, from our analysis of the 28-cm-long shoot, we find preliminary evidence for the possible role of non-growing season conditions in controlling the isotopic signatures of growth increments in the subsequent growing season, through direct plant use of snowmelt or snowmelt contributions to peatland hydrology. These processes imply that even environmental changes during the non-growing season cannot be simply overlooked, although this remains to be supported by more extensive field-based data. A few previous studies have informally considered the importance of non-growing season conditions when

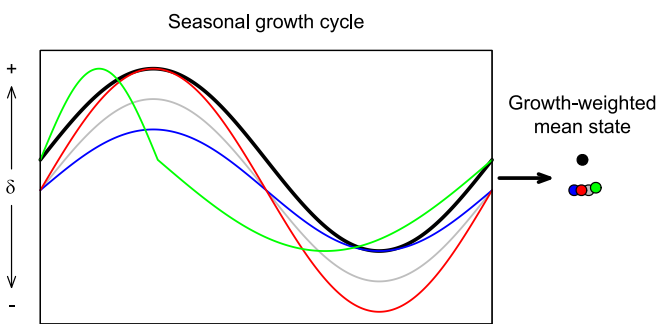


**Fig. 11.** Schematic diagram illustrating that lower “mean-state” values of *Sphagnum*  $\delta^{13}\text{C}$  and  $\delta^{18}\text{O}$  in peatland records can result from various processes: lower seasonal peaks (blue line), lower seasonal troughs (red line), lower peaks and troughs simultaneously (gray line), or a relative increase (decrease) in growth during isotopic trough (peak) periods (green line). (For interpretation of the references to colour in this figure legend, the reader is referred to the web version of this article.)

explaining their isotope-proxy records, which we believe to be totally plausible based on the findings of this study. For example, Willis et al. (2015) suggested that higher *Sphagnum*  $\delta^{13}\text{C}$  signals (indicating wetter conditions) during the generally drier Little Ice Age in West Siberia possibly resulted from the effect of delayed snowmelt on peatland water balance. Kaislahti Tillman et al. (2013) proposed, based on a study in the Arctic tundra, that higher winter precipitation  $\delta^{18}\text{O}$  due to changes in wintertime atmospheric circulation patterns may transmit into higher *Sphagnum*  $\delta^{18}\text{O}$  signals through the plant use of snowmelt.

Second, because *Sphagnum* moss growth itself is highly sensitive to the availability of energy (temperature and light), water (water table and precipitation), and nutrients (Clymo, 1970; Clymo and Hayward, 1982; Hayward and Clymo, 1983; Gerdol, 1995; Bengtsson et al., 2021), the wide range of isotopic variability in seasonal growth increments suggests that changes in the seasonal growth patterns of *Sphagnum* mosses, in response to environmental changes or under different climate conditions, may result in notable shifts in growth-weighted “mean-state”  $\delta^{13}\text{C}$  and  $\delta^{18}\text{O}$  values preserved and measured from peatland records (Fig. 11). Previous studies based on field growth measurements have found a diversity in the seasonal distribution of *Sphagnum* moss growth, with reports of more concentrated growth in summer (Clymo, 1970; Clymo and Hayward, 1982), in early and late growing seasons (Moore et al., 2002; Asada et al., 2003; Koronatova et al., 2022), or only in the early growing season (Kosykh et al., 2017). Some of these studies have also noted that seasonal growth patterns can shift between years due to different climate conditions (Moore, 1989; Lindholm, 1990; Genet et al., 2013). Considering the potential role of environment-growth interactions, our results support that shifts to lower “mean-state”  $\delta^{18}\text{O}$  values, for example, may result from environmentally driven, relatively increased (decreased) plant growth during seasons with lower (higher) precipitation  $\delta^{18}\text{O}$  relative to the annual production, and vice versa (Fig. 11). Our recent study in a peatland in northern Northeast China found a large-magnitude (6‰) negative (to lower values) excursion of *Sphagnum*  $\delta^{18}\text{O}$  spanning several decades during the 20th century, and interpreted this phenomenon as reflecting warming-driven summer desiccation that shifted biomass production to the period of cold seasons (with very low  $\delta^{18}\text{O}$ ) (Xia et al., 2024). In our analysis of the 28-cm-long shoot, we hypothesize another specific mechanism that the snowmelt signature of low  $\delta^{18}\text{O}$  can be registered into new growth increments as a distinct large-magnitude and long-duration  $\delta^{18}\text{O}$  trough during a warm late-winter and early-spring period (Fig. 7b). This mechanism has previously been considered by Daley et al. (2010) and Cleary et al. (2024) in interpreting their *Sphagnum*  $\delta^{18}\text{O}$  records.

Additionally, the seasonality fingerprint of isotopic proxies likely vary among different habitats or species. From the inconsistent shoot-specific isotopic variations between the 28-cm-long and 7-cm-long

shoots (Fig. 5), there is an absence of apparent seasonal patterns in the  $\delta^{13}\text{C}$  data for the 7-cm-long shoot inhabiting the moisture-limiting hummock top. This feature may reflect certain plant adaptations that enable self-regulation of local habitats, such as forming a compact and dense shoot structure with higher water retention capacity, lower evapotranspiration rates, and more effective capillary transport of water (Moore, 1989; Turetsky et al., 2008; Rydin and Jeglum, 2013; McCarter and Price, 2014). The habitat- or species-specific growth responses to environmental factors have been extensively investigated in the literature based on field growth measurements (Clymo, 1970; Clymo and Hayward, 1982; Gerdol, 1995; Laine et al., 2011; Bengtsson et al., 2021; Koronatova et al., 2022). Therefore, shifts in local habitats or species may also affect “mean-state”  $\delta^{13}\text{C}$  and  $\delta^{18}\text{O}$  values due to changing climate sensitivities and environment-growth interactions.

## 5. Concluding remarks

In this study, we present a unique dataset of *Sphagnum* cellulose  $\delta^{13}\text{C}$  and  $\delta^{18}\text{O}$  measurements that capture the full ranges of both spatial variations across local microtopographic gradients and temporal variations at sub-annual resolution from a peatland in Northeast China. The spatial dataset, derived from surface *Sphagnum* mosses, provides an independent confirmation of the “water film” effect on the  $\delta^{13}\text{C}$  signal and the evaporative enrichment effect on the  $\delta^{18}\text{O}$  signal, both of which are related to moisture availability and have been established in previous studies (e.g., Xia et al., 2020). The temporal dataset, derived from millimeter-scale sequential analysis of long *Sphagnum* moss shoots, reveals large-magnitude cyclic variations in  $\delta^{13}\text{C}$  and  $\delta^{18}\text{O}$  data, reflecting gradual seasonal shifts in moisture availability and plant source water  $\delta^{18}\text{O}$ , respectively. Compared to the spatial dataset, the magnitude of temporal variations is similar for  $\delta^{13}\text{C}$  and twice as large as for  $\delta^{18}\text{O}$ . There are distinguishable changes in the level or length of isotopic peaks and troughs that may result from changes in seasonal climate conditions and their effects on moss growth responses.

Together, our study highlights the need to appraise the influence of seasons, including both changes in seasonal climate and seasonal plant growth, when interpreting *Sphagnum*  $\delta^{13}\text{C}$  and  $\delta^{18}\text{O}$  proxies in peatland records. This new perspective reveals the limitations of the commonly adopted methodology of space-for-time substitution and may provide an avenue to reconcile, for example, the existing inconsistency in the pattern and magnitude of “mean-state” precipitation  $\delta^{18}\text{O}$  variations reconstructed from *Sphagnum*-dominated peatlands compared to open lake or speleothem archives (Constantin et al., 2007; Daley et al., 2009; Finkenbinder et al., 2016; Túri et al., 2021). However, we still have limited knowledge about how the sub-annual course of contemporary *Sphagnum* moss growth is regulated by seasonal climate conditions

across different geographical locations, peatland types, and local habitats (Clymo and Hayward, 1982; Moore, 1989; Moore et al., 2002; Laine et al., 2011; Küttim et al., 2020), because most available field growth measurements focus on annual growth rates (Loisel et al., 2012; Bengtsson et al., 2021; Koronatova et al., 2022). As the number of paleoenvironmental records has grown rapidly in recent years, discrepancies or conflicts among various records have become common, with varying seasonal sensitivities of different proxies or archives being invoked as one of the main causes (Steinman et al., 2012; Linderholm et al., 2018; Zhang et al., 2022). Therefore, understanding the seasonally resolved ecological processes and mechanisms that control *Sphagnum*  $\delta^{13}\text{C}$  and  $\delta^{18}\text{O}$  signatures will further support the development of proxy system models that allow for integrating these records into the framework of paleoclimate data assimilation (Dee et al., 2015; Erb et al., 2022) and peatland ecosystem modeling (Walker et al., 2017).

## CRediT authorship contribution statement

**Zhengyu Xia:** Visualization, Validation, Supervision, Resources, Project administration, Methodology, Investigation, Funding acquisition, Formal analysis, Data curation, Conceptualization, Writing – original draft. **Yueyan Jiang:** Visualization, Validation, Investigation, Formal analysis, Data curation, Writing – original draft. **Yingfan Xia:** Formal analysis, Data curation. **Meng Wang:** Data curation. **Shaoqing Zhang:** Data curation. **Zhao-Jun Bu:** Data curation. **Zicheng Yu:** Supervision, Resources, Project administration, Methodology, Investigation, Funding acquisition, Conceptualization, Writing – review & editing.

## Declaration of competing interest

The authors declare that they have no known competing financial interests or personal relationships that could have appeared to influence the work reported in this paper.

## Acknowledgments

We thank Julie Loisel (University of Nevada, Reno) for comments that have improved this manuscript, Camille Risi (Laboratoire de Météorologie Dynamique) for providing the recent LMDZ simulation outputs, Yu Pan for measuring *Sphagnum* growth rates in the field, Yuefeng Li for flying a drone to collect elevation data. This work was supported by the National Natural Science Foundation of China (42201167, 42494822), Fundamental Research Funds for the Central Universities (2412023YQ006 and 135112004), and Natural Science Foundation of Jilin Province (20230101077JC).

## Appendix A. Mathematical modeling of sub-annual isotopic variations in stems and branches of *Sphagnum* mosses

As mentioned in Section 3.2, stem  $\delta^{13}\text{C}$  and branch  $\delta^{13}\text{C}$  data from the 28-cm-long shoot exhibit different trough patterns. This appendix aims to use a mathematical model to demonstrate that these different trough patterns can be explained by their distinct growth processes. Briefly, stems elongate incrementally over time, and their isotopic variations along the shoot can be viewed as a simple continuous time series. Branches grow for an extended period, not only in capitula but also after being distributed to stems, until expanding into fully intact forms (Johansson and Linder, 1980; Aldous, 2002). Therefore, isotopic signals of individual branches tend to integrate growth conditions over a particular time window, mathematically similar to the moving average of isotopic time series recorded in stems.

We utilize the following “tilted” sine function to simulate cyclic time series that alternates between abrupt decreases and gradual increases of a variable over time:

$$\delta = a^{-1} \tan^{-1} \frac{\sin t}{1 - a \cos t} \quad (-1 < a < 0) \quad (\text{A1})$$

where  $\delta$  denotes the relative change in the isotopic composition ( $\delta^{13}\text{C}$  or  $\delta^{18}\text{O}$ ),  $a$  is a parameter that controls the shape of the function, and  $t$  is time. The function approximates to  $\delta = \sin t$  when  $a \rightarrow 0$  and to a polyline when  $a \rightarrow -1$ .

We set  $a = -0.8$  for Eq. A1 to generate a hypothetical time series of stem  $\delta^{13}\text{C}$  that reproduces the “mirrored check mark” shape of the trough pattern observed in our stem  $\delta^{13}\text{C}$  data (Fig. A1a). By doing so, we implicitly assume a constant rate of length increment and skip the time period in

winter when plant production completely stops. At a particular moment  $t$  when a new piece of stem section forms, the  $\delta^{13}\text{C}$  of a branch that is just isolated from the capitulum and attached to that stem can be expressed as follows:

$$\delta_b(t) = \frac{1}{\Delta t} \int_{t-x\Delta t}^{t+(1-x)\Delta t} \delta_s(t) dt \quad (\text{A2})$$

where  $\delta_b$  and  $\delta_s$  refer to branch  $\delta^{13}\text{C}$  and stem  $\delta^{13}\text{C}$ , respectively,  $\Delta t$  is the timespan of branch growth, and  $x$  is the proportion of branch growth that precedes stem formation (thus  $1-x$  indicates the proportion of branch growth occurring after stem formation). After several trials, we set  $\Delta t = 0.4 \times 2\pi$  and  $x = 0.8$ , implying that the timespan for a branch to fully grow lasts for 40 % time of a yearly cycle, with 80 % of that growth occurring in the capitulum before being distributed to the stem. The results reproduce the “V” shape of the trough pattern observed in our branch  $\delta^{13}\text{C}$  data, as well as their reduced amplitude of variability compared to stem  $\delta^{13}\text{C}$  (Fig. A1a).

However, our branch  $\delta^{18}\text{O}$  data exhibit the same pattern of variations as stem  $\delta^{18}\text{O}$ , with abrupt decreases followed by gradual decreases (Fig. 7b), and are not affected by the “moving average” effect. A simple possible mechanism is that  $\delta^{18}\text{O}$  signals are fingerprinted during cellulose synthesis over a narrower time window, whereas  $\delta^{13}\text{C}$  signals are fingerprinted by sucrose sources produced by photosynthesis over a wider time window. As an illustration, we create another suite of hypothetical time series for stem  $\delta^{18}\text{O}$  and branch  $\delta^{18}\text{O}$  by setting  $\Delta t = 0.2 \times 2\pi$  and keeping other parameters the same. The results can reproduce the observed pattern shown in our data, including the similar amplitude of variability between stem  $\delta^{18}\text{O}$  and branch  $\delta^{18}\text{O}$  (Fig. A1b).

The simple mathematical modeling we present does not consider detailed ecological processes, such as growth rate, production and storage of sucrose, and turnover of plant-associated water, which vary seasonally and may affect isotopic signatures in growth increments. A realistic representation of these processes necessitates a process-based, mechanistic model that can simulate the photosynthesis and growth of *Sphagnum* mosses (Hayward and Clymo, 1983; Williams and Flanagan, 1998; Walker et al., 2017).

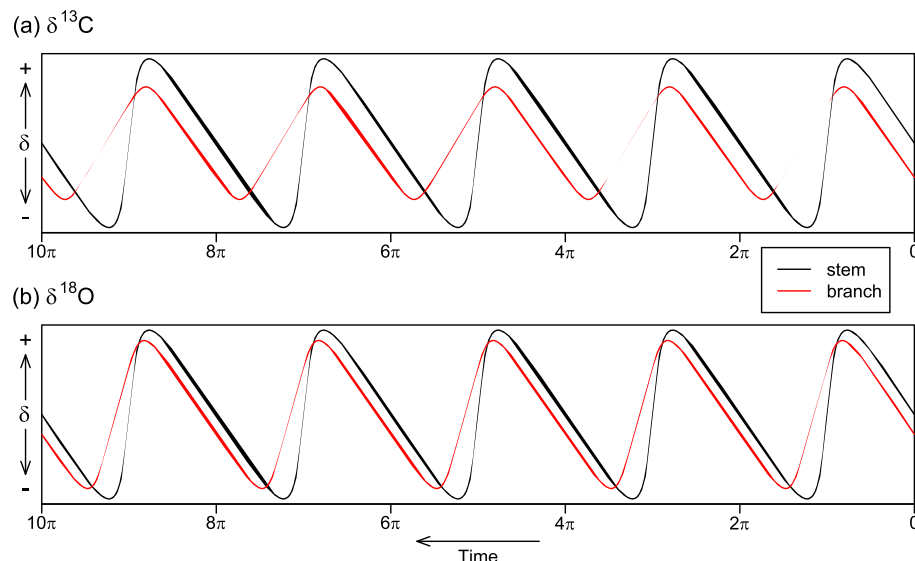


**Fig. A1.** Hypothetical time series of (a)  $\delta^{13}\text{C}$  and (b)  $\delta^{18}\text{O}$  for stems (black lines) and branches (red lines) simulated by the “tilted” sine function. (For interpretation of the references to colour in this figure legend, the reader is referred to the web version of this article.)

## Appendix B. Modeled isotopic composition of precipitation

Since we did not collect precipitation samples in preceding years, and there is no local station monitoring the isotopic composition of precipitation, we chose to use the available output of a nudged isotope-enabled GCM LMDZ4 (Risi et al., 2010) to estimate the monthly precipitation  $\delta^{18}\text{O}$  at the grid of our site during the period of interest. LMDZ4 is the most accurate GCM in the second phase of the Stable Water Isotope Intercomparison Group (SWING2) for simulating precipitation isotopes in China (Risi et al., 2012; Che et al., 2016; Yang et al., 2017). At our site, it can well reproduce the 12-monthly climatological mean precipitation  $\delta^{18}\text{O}$  provided by the observation-based geostatistical model Online Isotopes in Precipitation Calculator (OIPC; Bowen et al., 2005).

## Appendix C. Supplementary data

Supplementary data to this article can be found online at <https://doi.org/10.1016/j.palaeo.2025.113269>.

## Data availability

Raw isotope data presented in this study are available on Figshare at: <https://doi.org/10.6084/m9.figshare.25670709.v1>

## References

- Aldous, A.R., 2002. Nitrogen translocation in *Sphagnum* mosses: Effects of atmospheric nitrogen deposition. *New Phytol.* 156 (2), 241–253.
- Amesbury, M.J., Charman, D.J., Newnham, R.M., Loader, N.J., Goodrich, J., Royles, J., Campbell, D.I., Keller, E.D., Baisden, W.T., Roland, T.P., Gallego-Sala, A.V., 2015a. Can oxygen stable isotopes be used to track precipitation moisture source in vascular plant-dominated peatlands? *Earth Planet. Sci. Lett.* 430, 149–159.

- Amesbury, M.J., Charman, D.J., Newnham, R.M., Loader, N.J., Goodrich, J.P., Royles, J., Campbell, D.I., Roland, T.P., Gallego-Sala, A., 2015b. Carbon stable isotopes as a palaeoclimate proxy in vascular plant dominated peatlands. *Geochim. Cosmochim. Acta* 164, 161–174.
- Aravena, R., Warner, B.G., 1992. Oxygen-18 composition of *Sphagnum*, and microenvironmental water Relations. *The Bryologist* 95 (4), 445–448.
- Asada, T., Warner, B.G., Banner, A., 2003. Growth of mosses in relation to climate factors in a hypermaritime coastal peatland in British Columbia, Canada. *The Bryologist* 106 (4), 516–527.
- Barber, K.E., Chambers, F.M., Maddy, D., 2003. Holocene palaeoclimates from peat stratigraphy: Macrofossil proxy climate records from three oceanic raised bogs in England and Ireland. *Quat. Sci. Rev.* 22 (5), 521–539.
- Bengtsson, F., Rydin, H., Baltzer, J.L., Bragazza, L., Bu, Z.-J., Caporn, S.J.M., Dorrepaal, E., Flatberg, K.I., Galanina, O., Gałka, M., Ganeva, A., Goia, I., Goncharova, N., Hájek, M., Haraguchi, A., Harris, L.I., Humphreys, E., Jirousek, M., Kajukalo, K., Karofeld, E., Koronatova, N.G., Kosykh, N.P., Laine, A.M., Lamentowicz, M., Lapshina, E., Limpens, J., Linkosalmi, M., Ma, J.-Z., Mauritz, M., Mitchell, E.A.D., Munir, T.M., Natali, S.M., Natcheva, R., Payne, R.J., Philippov, D. A., Rice, S.K., Robinson, S., Robroek, B.J.M., Rochefort, L., Singer, D., Stenøien, H.K., Tuittila, E.-S., Vellak, K., Waddington, J.M., Granath, G., 2021. Environmental drivers of *Sphagnum* growth in peatlands across the Holarctic region. *J. Ecol.* 109 (1), 417–431.
- Booth, R.K., 2002. Testate amoebae as paleoindicators of surface-moisture changes on Michigan peatlands: Modern ecology and hydrological calibration. *J. Paleolimnol.* 28 (3), 329–348.
- Booth, R.K., Notaro, M., Jackson, S.T., Kutzbach, J.E., 2006. Widespread drought episodes in the western Great Lakes region during the past 2000 years: Geographic extent and potential mechanisms. *Earth Planet. Sci. Lett.* 242 (3), 415–427.
- Bowen, G.J., 2008. Spatial analysis of the intra-annual variation of precipitation isotope ratios and its climatological corollaries. *J. Geophys. Res.* 113, D05113.
- Bowen, G.J., Wassenaar, I.L., Hobson, K.A., 2005. Global application of stable hydrogen and oxygen isotopes to wildlife forensics. *Oecologia* 143 (3), 337–348.
- Brader, A.V., van Winden, J.F., Bohncke, S.J.P., Beets, C.J., Reichart, G.-J., de Leeuw, J. W., 2010. Fractionation of hydrogen, oxygen and carbon isotopes in *n*-alkanes and cellulose of three *Sphagnum* species. *Org. Geochem.* 41 (12), 1277–1284.
- Brenninkmeijer, C.A.M., van Geel, B., Mook, W.G., 1982. Variations in the D/H and  $^{18}\text{O}/^{16}\text{O}$  ratios in cellulose extracted from a peat bog core. *Earth Planet. Sci. Lett.* 61 (2), 283–290.
- Bu, Z.-J., Rydin, H., Chen, X., 2011. Direct and interaction-mediated effects of environmental changes on peatland bryophytes. *Oecologia* 166 (2), 555–563.
- Chambers, F.M., Booth, R.K., De Vleeschouwer, F., Lamentowicz, M., Le Roux, G., Mauquoy, D., Nichols, J.E., van Geel, B., 2012. Development and refinement of proxy-climate indicators from peats. *Quat. Int.* 268, 21–33.
- Che, Y., Zhang, M., Wang, S., Wang, J., Liu, Y., Zhang, F., 2016. Stable water isotopes of precipitation in China simulated by SWING2 models. *Arab. J. Geosci.* 9 (19), 732.
- Cleary, K.G., Xia, Z., Yu, Z., 2024. The growth and carbon sink of tundra peat patches in Arctic Alaska. *J. Geophys. Res. Biogeosci.* 129 (6) e2023JG007890.
- Clymo, R.S., 1970. The growth of *Sphagnum*: Methods of measurement. *J. Ecol.* 58 (1), 13–49.
- Clymo, R.S., Hayward, P.M., 1982. The Ecology of *Sphagnum*. In: Smith, A.J.E. (Ed.), *Bryophyte Ecology*. Springer, Netherlands, Dordrecht, pp. 229–289.
- Constantin, S., Bojar, A.-V., Lauritzen, S.-E., Lundberg, J., 2007. Holocene and late Pleistocene climate in the sub-Mediterranean continental environment: a speleothem record from Poleva Cave (Southern Carpathians, Romania). *Palaeogeogr. Palaeoclimatol. Palaeoecol.* 243 (3), 322–338.
- Daley, T.J., Street-Perrott, F.A., Loader, N.J., Barber, K.E., Hughes, P.D.M., Fisher, E.H., Marshall, J.D., 2009. Terrestrial climate signal of the “8200 yr B.P. Cold event” in the Labrador Sea region. *Geology* 37 (9), 831–834.
- Daley, T.J., Barber, K.E., Street-Perrott, F.A., Loader, N.J., Marshall, J.D., Crowley, S.F., Fisher, E.H., 2010. Holocene climate variability revealed by oxygen isotope analysis of *Sphagnum* cellulose from Walton Moss, northern England. *Quat. Sci. Rev.* 29 (13), 1590–1601.
- Dansgaard, W., 1964. Stable isotopes in precipitation. *Tellus* 16 (4), 436–468.
- Dee, S., Emile-Geay, J., Evans, M.N., Allam, A., Steig, E.J., Thompson, D.M., 2015. PRYSM: an open-source framework for PROXy System Modeling, with applications to oxygen-isotope systems. *J. Adv. Model. Earth Syst.* 7 (3), 1220–1247.
- Dorrepaal, E., Aerts, R., Cornelissen, J.H.C., Callaghan, T.V., Van Logtestijn, R.S.P., 2004. Summer warming and increased winter snow cover affect *Sphagnum fuscum* growth, structure and production in a sub-arctic bog. *Glob. Chang. Biol.* 10 (1), 93–104.
- Erb, M.P., McKay, N.P., Steiger, N., Dee, S., Hancock, C., Ivanovic, R.F., Gregoire, L.J., Valdes, P., 2022. Reconstructing Holocene temperatures in time and space using paleoclimate data assimilation. *Clim. Past* 18 (12), 2599–2629.
- Farquhar, G.D., Ehleringer, J.R., Hubick, K.T., 1989. Carbon isotope discrimination and photosynthesis. *Annu. Rev. Plant. Physiol. Plant. Mol. Biol.* 40 (1), 503–537.
- Finkenbinder, M.S., Abbott, M.B., Steinman, B.A., 2016. Holocene climate change in Newfoundland reconstructed using oxygen isotope analysis of lake sediment cores. *Global Planet. Change* 143, 251–261.
- Garcin, Y., Schefuß, E., Dargie, G.C., Hawthorne, D., Lawson, I.T., Sebag, D., Biddulph, G. E., Crezee, B., Bocko, Y.E., Ifo, S.A., Mampouya Wenina, Y.E., Mbemba, M., Ewango, C.E.N., Emba, O., Bola, P., Kanya Tabu, J., Tyrrell, G., Young, D.M., Gassier, G., Girkin, N.T., Vane, C.H., Adatte, T., Baird, A.J., Boom, A., Gulliver, P., Morris, P.J., Page, S.E., Sjögersten, S., Lewis, S.L., 2022. Hydroclimatic vulnerability of peat carbon in the Central Congo Basin. *Nature* 612 (7939), 277–282.
- Genet, H., Oberbauer, S.F., Colby, S.J., Staudhammer, C.L., Starr, G., 2013. Growth responses of *Sphagnum* hollows to a growing season lengthening manipulation in Alaskan Arctic tundra. *Polar Biol.* 36 (1), 41–50.
- Gerdol, R., 1995. The growth dynamics of *Sphagnum* based on field measurements in a temperate bog and on laboratory cultures. *J. Ecol.* 83 (3), 431–437.
- Granath, G., Rydin, H., Baltzer, J.L., Bengtsson, F., Boncek, N., Bragazza, L., Bu, Z.J., Caporn, S.J.M., Dorrepaal, E., Galanina, O., Gałka, M., Ganeva, A., Gillikin, D.P., Goia, I., Goncharova, N., Hájek, M., Haraguchi, A., Harris, L.I., Humphreys, E., Jirousek, M., Kajukalo, K., Karofeld, E., Koronatova, N.G., Kosykh, N.P., Lamentowicz, M., Lapshina, E., Limpens, J., Linkosalmi, M., Ma, J.Z., Mauritz, M., Munir, T.M., Natali, S.M., Natcheva, R., Noskova, M., Payne, R.J., Pilkington, K., Robinson, S., Robroek, B.J.M., Rochefort, L., Singer, D., Stenøien, H.K., Tuittila, E.S., Vellak, K., Verheyden, A., Waddington, J.M., Rice, S.K., 2018. Environmental and taxonomic controls of carbon and oxygen stable isotope composition in *Sphagnum* across broad climatic and geographic ranges. *Biogeoosci* 15 (16), 5189–5202.
- Hayward, P.M., Clymo, R.S., 1983. The growth of *Sphagnum*: experiments on, and simulation of, some effects of light flux and water-table depth. *J. Ecol.* 71 (3), 845–863.
- Hong, Y.T., Hong, B., Lin, Q.H., Shibata, Y., Hirota, M., Zhu, Y.X., Leng, X.T., Wang, Y., Wang, H., Yi, L., 2005. Inverse phase oscillations between the East Asian and Indian Ocean summer monsoons during the last 12000 years and paleo-El Niño. *Earth Planet. Sci. Lett.* 231 (3), 337–346.
- Huang, X., Xue, J., Meyers, P.A., Gong, L., Wang, X., Liu, Q., Qin, Y., Wang, H., 2014. Hydrologic influence on the  $\delta^{13}\text{C}$  variation in long chain *n*-alkanes in the Dajiuhan peatland, Central China. *Org. Geochem.* 69, 114–119.
- Huang, X., Pancost, R.D., Xue, J., Gu, Y., Evershed, R.P., Xie, S., 2018. Response of carbon cycle to drier conditions in the mid-Holocene in Central China. *Nat. Commun.* 9 (1), 1369.
- Johansson, L.G., Linder, S., 1980. Photosynthesis of *Sphagnum* in different microhabitats on a subarctic mire. In: Sonesson, M. (Ed.), *Ecology of a Subarctic Mire*. Ecological Bulletins. Oikos Editorial Office, Stockholm, Sweden, pp. 181–190.
- Jouzel, J., Hoffmann, G., Koster, R.D., Masson, V., 2000. Water isotopes in precipitation: data/model comparison for present-day and past climates. *Quat. Sci. Rev.* 19 (1), 363–379.
- Kaislahti Tillman, P., Holzkämper, S., Kuhrý, P., Sannel, A.B.K., Loader, N.J., Robertson, I., 2010a. Stable carbon and oxygen isotopes in *Sphagnum fuscum* peat from subarctic Canada: Implications for palaeoclimate studies. *Chem. Geol.* 270 (1), 216–226.
- Kaislahti Tillman, P., Holzkämper, S., Kuhrý, P., Sannel, A.B.K., Loader, N.J., Robertson, I., 2010b. Long-term climate variability in continental subarctic Canada: a 6200-year record derived from stable isotopes in peat. *Palaeogeogr. Palaeoclimatol. Palaeoecol.* 298 (3), 235–246.
- Kaislahti Tillman, P., Holzkämper, S., Andersen, T.J., Hugelius, G., Kuhrý, P., Oksanen, P., 2013. Stable isotopes in *Sphagnum fuscum* peat as late-Holocene climate proxies in northeastern European Russia. *The Holocene* 23 (10), 1381–1390.
- Koronatova, N.G., Kosykh, N.P., Saib, E.A., Stepanova, V.A., Vishnyakova, E.K., Granath, G., 2022. Weather factors in different growing periods determine inter-annual change in growth of four *Sphagnum* species: evidence from an eight-year study. *Wetlands* 42 (8), 118.
- Kosykh, N.P., Koronatova, N.G., Granath, G., 2017. Effect of temperature and precipitation on linear increment of *Sphagnum fuscum* and *S. magellanicum* in Western Siberia. *Russ. J. Ecol.* 48 (3), 203–211.
- Küttim, M., Küttim, L., Ilomets, M., Laine, A.M., 2020. Controls of *Sphagnum* growth and the role of winter. *Ecol. Res.* 35 (1), 219–234.
- Laine, A.M., Juurula, E., Hájek, T., Tuittila, E.-S., 2011. *Sphagnum* growth and ecophysiology during mire succession. *Oecologia* 167 (4), 1115–1125.
- Linderholm, H.W., Nicolle, M., Francus, P., Gajewski, K., Helama, S., Korhola, A., Solomin, O., Yu, Z., Zhang, P., D’Andrea, W.J., Debret, M., Divine, D.V., Gunnarson, B.E., Loader, N.J., Massei, N., Seftigen, K., Thomas, E.K., Werner, J., Andersson, S., Bernthsson, A., Luoto, T.P., Nevalainen, L., Saarni, S., Välijärvi, M., 2018. Arctic hydroclimate variability during the last 2000 years: current understanding and research challenges. *Clim. Past* 14 (4), 473–514.
- Lindholm, T., 1990. Growth dynamics of the peat moss *Sphagnum fuscum* on hummocks on a raised bog in southern Finland. *Ann. Bot. Fenn.* 27 (1), 67–78.
- Loader, N.J., Robertson, I., Barker, A.C., Switsur, V.R., Waterhouse, J.S., 1997. An improved technique for the batch processing of small wholewood samples to  $\alpha$ -cellulose. *Chem. Geol.* 136 (3), 313–317.
- Loader, N.J., McCarroll, D., van der Knaap, W.O., Robertson, I., Gagen, M., 2007. Characterizing carbon isotopic variability in *Sphagnum*. *The Holocene* 17 (3), 403–410.
- Loader, N.J., Street-Perrott, F.A., Mauquoy, D., Roland, T.P., van Bellen, S., Daley, T.J., Davies, D., Hughes, P.D.M., Pancotto, V.O., Young, G.H.F., Amesbury, M.J., Charman, D.J., Mallon, G., Yu, Z.C., 2016. Measurements of hydrogen, oxygen and carbon isotope variability in *Sphagnum* moss along a micro-topographical gradient in a southern Patagonian peatland. *J. Quat. Sci.* 31 (4), 426–435.
- Loisel, J., Garneau, M., Hélie, J.-F., 2009. Modern *Sphagnum*  $\delta^{13}\text{C}$  signatures follow a surface moisture gradient in two boreal peat bogs, James Bay lowlands. *Québec. J. Quat. Sci.* 24 (3), 209–214.
- Loisel, J., Garneau, M., Hélie, J.-F., 2010. *Sphagnum*  $\delta^{13}\text{C}$  values as indicators of palaeohydrological changes in a peat bog. *The Holocene* 20 (2), 285–291.
- Loisel, J., Gallego-Sala, A.V., Yu, Z., 2012. Global-scale pattern of peatland *Sphagnum* growth driven by photosynthetically active radiation and growing season length. *Biogeoosci* 9 (7), 2737–2746.
- Loisel, J., Sarna, K., Xia, Z., Huang, Y., Yu, Z., 2023. Concordant changes in late Holocene hydroclimate across southern Patagonia modulated by westerly winds and the El Niño–Southern Oscillation. *Geology* 51 (3), 247–251.
- Luken, J.O., 1985. Zonation of *Sphagnum* mosses: Interactions among shoot growth, growth form, and water balance. *Bryologist* 88 (4), 374–379.

- Markel, E.R., Booth, R.K., Qin, Y., 2010. Testate amoebae and  $\delta^{13}\text{C}$  of *Sphagnum* as surface-moisture proxies in Alaskan peatlands. *The Holocene* 20 (3), 463–475.
- Marschall, M., 2010. Photosynthetic responses, carbohydrate composition and invertase activity in fructan accumulating bryophytes (*Porella platyphylla* and *Sphagnum flexuosum*) under different environmental conditions (carbohydrate treatments, dark starvation, low temperature, desiccation). *Acta Biol. Hung.* 61, 120–129.
- McCarter, C.P.R., Price, J.S., 2014. Ecohydrology of *Sphagnum* moss hummocks: Mechanisms of capitula water supply and simulated effects of evaporation. *Ecohydrology* 7 (1), 33–44.
- McDermott, F., Matthey, D.P., Hawkesworth, C., 2001. Centennial-scale Holocene climate variability revealed by a high-resolution speleothem  $\delta^{18}\text{O}$  record from SW Ireland. *Science* 294 (5545), 1328–1331.
- Ménot, G., Burns, S.J., 2001. Carbon isotopes in ombrogenic peat bog plants as climatic indicators: Calibration from an altitudinal transect in Switzerland. *Org. Geochem.* 32 (2), 233–245.
- Ménot-Combes, G., Burns, S.J., Leuenberger, M., 2002. Variations of  $^{18}\text{O}/^{16}\text{O}$  in plants from temperate peat bogs (Switzerland): Implications for paleoclimatic studies. *Earth Planet. Sci. Lett.* 202 (2), 419–434.
- Moore, T.R., 1989. Growth and net production of *Sphagnum* at five fen sites, subarctic eastern Canada. *Can. J. Bot.* 67 (4), 1203–1207.
- Moore, T.R., Bubier, J.L., Froliking, S.E., Lafleur, P.M., Roulet, N.T., 2002. Plant biomass and production and  $\text{CO}_2$  exchange in an ombrotrophic bog. *J. Ecol.* 90 (1), 25–36.
- Moore, T.R., Lafleur, P.M., Poon, D.M.I., Heumann, B.W., Seaquist, J.W., Roulet, N.T., 2006. Spring photosynthesis in a cool temperate bog. *Glob. Chang. Biol.* 12 (12), 2323–2335.
- Moschen, R., Kühl, N., Peters, S., Vos, H., Lücke, A., 2011. Temperature variability at Dürres Maar, Germany during the Migration Period and at High medieval Times, inferred from stable carbon isotopes of *Sphagnum* cellulose. *Clim. Past* 7 (3), 1011–1026.
- Naafs, B.D.A., Inglis, G.N., Zheng, Y., Amesbury, M.J., Biester, H., Bindler, R., Blewett, J., Burrows, M.A., del Castillo Torres, D., Chambers, F.M., Cohen, A.D., Evershed, R.P., Feakins, S.J., Galka, M., Gallego-Sala, A., Gandois, L., Gray, D.M., Hatcher, P.G., Honorio Coronado, E.N., Hughes, P.D.M., Huguet, A., Könönen, M., Laggoun-Défarge, F., Lähteenoja, O., Lamontowicz, M., Marchant, R., McLymont, E., Pontevedra-Pombal, X., Ponton, C., Pourmand, A., Rizzuti, A.M., Rochelefort, L., Schellekens, J., De Vleeschouwer, F., Pancost, R.D., 2017. Introducing global peat-specific temperature and pH calibrations based on brGDGT bacterial lipids. *Geochim. Cosmochim. Acta* 208, 285–301.
- Nichols, J.E., Walcott, M., Bradley, R., Pilcher, J., Huang, Y., 2009. Quantitative assessment of precipitation seasonality and summer surface wetness using ombrotrophic sediments from an Arctic Norwegian peatland. *Quatern. Res.* 72 (3), 443–451.
- Norby, R.J., Childs, J., Hanson, P.J., Warren, J.M., 2019. Rapid loss of an ecosystem engineer: *Sphagnum* decline in an experimentally warmed bog. *Ecol. Evol.* 9 (22), 12571–12585.
- Ooki, S., Akagi, T., Jinno, H., Franzén, L.G., Newton, J., 2018. Hydrological study of Lyngmossen bog, Sweden: Isotopic tracers ( $^3\text{H}$ ,  $^{2\text{H}}$  and  $^{18}\text{O}$ ) imply three waters with different mobilities. *Quat. Sci. Rev.* 199, 97–107.
- Price, G.D., McKenzie, J.E., Pilcher, J.R., Hoper, S.T., 1997. Carbon-isotope variation in *Sphagnum* from hummock-hollow complexes: Implications for Holocene climate reconstruction. *The Holocene* 7 (2), 229–233.
- Proctor, M.C.F., Raven, J.A., Rice, S.K., 1992. Stable carbon isotope discrimination measurements in *Sphagnum* and other bryophytes: Physiological and ecological implications. *J. Bryol.* 17 (2), 193–202.
- Raghoebarsing, A.A., Smolders, A.J.P., Schmid, M.C., Rijpstra, W.I.C., Wolters-Arts, M., Derksen, J., Jetten, M.S.M., Schouten, S., Sinnighe Damsté, J.S., Lamers, L.P.M., Roelofs, J.G.M., Op den Camp, H.J.M., Strous, M., 2005. Methanotropic symbionts provide carbon for photosynthesis in peat bogs. *Nature* 436 (7054), 1153–1156.
- Rice, S.K., 2000. Variation in carbon isotope discrimination within and among *Sphagnum* species in a temperate wetland. *Oecologia* 123 (1), 1–8.
- Rice, S.K., Giles, L., 1996. The influence of water content and leaf anatomy on carbon isotope discrimination and photosynthesis in *Sphagnum*. *Plant Cell Environ.* 19 (1), 118–124.
- Risi, C., Bony, S., Vimeux, F., Jouzel, J., 2010. Water-stable isotopes in the LMDZ4 general circulation model: model evaluation for present-day and past climates and applications to climatic interpretations of tropical isotopic records. *J. Geophys. Res.* 115, D12118.
- Risi, C., Noone, D., Worden, J., Frankenberg, C., Stiller, G., Kiefer, M., Funke, B., Walker, K., Bernath, P., Schneider, M., Wunch, D., Sherlock, V., Deutscher, N., Griffith, D., Wennberg, P.O., Strong, K., Smale, D., Mahieu, E., Barthlott, S., Hase, F., García, O., Notholt, J., Warneke, T., Toon, G., Sayres, D., Bony, S., Lee, J., Brown, D., Uemura, R., Sturm, C., 2012. Process-evaluation of tropospheric humidity simulated by general circulation models using water vapor isotopologues: 1. Comparison between models and observations. *J. Geophys. Res.* 117, D05303.
- Robinson, S.A., King, D.H., Bramley-Alves, J., Waterman, M.J., Ashcroft, M.B., Wasley, J., Turnbull, J.D., Miller, R.E., Ryan-Colton, E., Benny, T., Mullany, K., Clarke, L.J., Barry, L.A., Hua, Q., 2018. Rapid change in East Antarctic terrestrial vegetation in response to regional drying. *Nat. Clim. Chang.* 8 (10), 879–884.
- Royles, J., Young, S., Griffiths, H., 2022. Stable isotope signals provide seasonal climatic markers for moss functional groups. *Proc. R. Soc. B* 289 (1967), 20212470.
- Rydin, H., Jeglum, J.K., 2013. The Biology of Peatlands, Second edition. Oxford University Press, Oxford, UK.
- Rydin, H., McDonald, A.J.S., 1985. Photosynthesis in *Sphagnum* at different water contents. *J. Bryol.* 13 (4), 579–584.
- Schröder, C., Thiele, A., Wang, S., Bu, Z., Joosten, H., 2007. Hani-mire: a percolation mire in Northeast China. *Peatlands International* 2, 21–24.
- Serk, H., Nilsson, M.B., Bohlin, E., Ehlers, I., Wieloch, T., Olid, C., Grover, S., Kalbitz, K., Limpens, J., Moore, T., Münchberger, W., Talbot, J., Wang, X., Knorr, K.-H., Pancotto, V., Schleucher, J., 2021. Global  $\text{CO}_2$  fertilization of *Sphagnum* peat mosses via suppression of photorespiration during the twentieth century. *Sci. Rep.* 11 (1), 24517.
- Shi, F., Rao, Z., Cao, J., Huang, C., Wu, D., Yang, W., Sun, W., 2019. Meltwater is the dominant water source controlling  $\alpha$ -cellulose  $\delta^{18}\text{O}$  in a vascular-plant-dominated alpine peatland in the Altai Mountains, Central Asia. *J. Hydrol.* 572, 192–205.
- Skrzypek, G., Kalužny, A., Wojtuń, B., Jędrysek, M.-O., 2007. The carbon stable isotopic composition of mosses: a record of temperature variation. *Org. Geochem.* 38 (10), 1770–1781.
- Steinman, B.A., Abbott, M.B., Mann, M.E., Stansell, N.D., Finney, B.P., 2012. 1,500 year quantitative reconstruction of winter precipitation in the Pacific Northwest. *Proc. Natl. Acad. Sci. U. S. A.* 109 (29), 11619–11623.
- Sternberg, L.D.S.L., Deniro, M.J., Savidge, R.A., 1986. Oxygen isotope exchange between metabolites and water during biochemical reactions leading to cellulose synthesis. *Plant Physiol.* 82 (2), 423–427.
- Swindles, G.T., Morris, P.J., Mullan, D.J., Payne, R.J., Roland, T.P., Amesbury, M.J., Lamontowicz, M., Turner, T.E., Gallego-Sala, A., Sim, T., Barr, I.D., Blaauw, M., Blundell, A., Chambers, F.M., Charman, D.J., Feurdean, A., Galloway, J.M., Galka, M., Green, S.M., Kajukalo, K., Karofeld, E., Korhola, A., Lamontowicz, E., Langdon, P., Marcisz, K., Mauquoy, D., Mazei, Y.A., McKeown, M.M., Mitchell, E.A. D., Novenko, E., Plunkett, G., Roe, H.M., Schonung, K., Sillasoo, Ü., Tsyanov, A.N., van der Linden, M., Välijarva, M., Warner, B., 2019. Widespread drying of European peatlands in recent centuries. *Nat. Geosci.* 12 (11), 922–928.
- Turetsky, M.R., Crow, S.E., Evans, R.J., Vitt, D.H., Wieder, R.K., 2008. Trade-offs in resource allocation among moss species control decomposition in boreal peatlands. *J. Ecol.* 96 (6), 1297–1305.
- Túri, M., Hubay, K., Molnár, M., Braun, M., László, E., Futó, I., Pálcsu, L., 2021. Holocene paleoclimate inferred from stable isotope ( $\delta^{18}\text{O}$  and  $\delta^{13}\text{C}$ ) values in *Sphagnum* cellulose, Mohos peat bog, Romania. *J. Paleolimnol.* 66 (3), 229–248.
- Turney, C.S.M., Kershaw, A.P., Clemens, S.C., Branch, N., Moss, P.T., Keith Fifield, L., 2004. Millennial and orbital variations of El Niño/Southern Oscillation and high-latitude climate in the last glacial period. *Nature* 428 (6980), 306–310.
- UNEP, 2022. Global Peatlands Assessment: The State of the World's Peatlands. United Nations Environment Programme, Nairobi, Kenya.
- Walker, A.P., Carter, K.R., Gu, L., Hanson, P.J., Malhotra, A., Norby, R.J., Sebestyen, S. D., Wullschleger, S.D., Weston, D.J., 2017. Biophysical drivers of seasonal variability in *Sphagnum* gross primary production in a northern temperate bog. *J. Geophys. Res. Biogeosci.* 122 (5), 1078–1097.
- Wang, M., Tian, J., Bu, Z., Lamit, L.J., Chen, H., Zhu, Q., Peng, C., 2019. Structural and functional differentiation of the microbial community in the surface and subsurface peat of two minerotrophic fens in China. *Plant and Soil* 437 (1), 21–40.
- Williams, T.G., Flanagan, L.B., 1996. Effect of changes in water content on photosynthesis, transpiration and discrimination against  $^{13}\text{CO}_2$  and  $^{18}\text{O}^{16}\text{O}$  in *Pleurozium* and *Sphagnum*. *Oecologia* 108 (1), 38–46.
- Williams, T.G., Flanagan, L.B., 1998. Measuring and modelling environmental influences on photosynthetic gas exchange in *Sphagnum* and *Pleurozium*. *Plant Cell Environ.* 21 (6), 555–564.
- Willis, K.S., Beilmann, D., Booth, R.K., Amesbury, M., Holmquist, J., MacDonald, G., 2015. Peatland paleohydrology in the southern West Siberian Lowlands: Comparison of multiple testate amoeba transfer functions, sites, and *Sphagnum*  $\delta^{13}\text{C}$  values. *The Holocene* 25 (9), 1425–1436.
- Xia, Z., Yu, Z., 2020. Temperature-dependent oxygen isotope fractionation in plant cellulose biosynthesis revealed by a global dataset of peat mosses. *Front. Earth Sci.* 8.
- Xia, Z., Yu, Z., Loisel, J., 2018. Centennial-scale dynamics of the Southern Hemisphere Westerly Winds across the Drake Passage over the past two millennia. *Geology* 46 (10), 855–858.
- Xia, Z., Zheng, Y., Stelling, J.M., Loisel, J., Huang, Y., Yu, Z., 2020. Environmental controls on the carbon and water (H and O) isotopes in peatland *Sphagnum* mosses. *Geochim. Cosmochim. Acta* 277, 265–284.
- Xia, Z., Yang, W., Yu, Z., 2024. Major moisture shifts in inland Northeast Asia during the last millennium. *Environ. Res. Lett.* 19 (12), 124005.
- Xia, Y., Xia, Z., Yu, Z., 2025. A 1700-year peatland-based hydroclimate record from the Hengduan Mountains in the southeastern Tibetan Plateau reveals changing dynamics of the summer monsoon interface. *Quat. Sci. Rev.* 366, 109501.
- Xie, S., Evershed, R.P., Huang, X., Zhu, Z., Pancost, R.D., Meyers, P.A., Gong, L., Hu, C., Huang, J., Zhang, S., Gu, Y., Zhu, J., 2013. Concordant monsoon-driven postglacial hydrological changes in peat and stalagmite records and their impacts on prehistoric cultures in Central China. *Geology* 41 (8), 827–830.
- Yang, S., Zhang, M., Wang, S., Liu, Y., Qiang, F., Qu, D., 2017. Interannual trends in stable oxygen isotope composition in precipitation of China during 1979–2007: Spatial incoherence. *Quat. Int.* 454, 25–37.
- Yasuda, S., Ooki, S., Naraoaka, H., Akagi, T., 2015. Carbon isotopes in *Sphagnum* from Kyushu, Japan, and their relationship with local climate. *Geochem. J.* 49 (5), 495–502.
- Zanazzi, A., Mora, G., 2005. Paleoclimatic implications of the relationship between oxygen isotope ratios of moss cellulose and source water in wetlands of Lake Superior. *Chem. Geol.* 222 (3), 281–291.
- Zhang, Q., Hu, Z., 2018. Assessment of drought during corn growing season in Northeast China. *Theor. Appl. Climatol.* 133 (3), 1315–1321.
- Zhang, Z., Cao, Y., Wang, T., Bambalov, N.N., 1997. Comparative study on origin and development feature of peat mire. *Journal of Northeast Normal University* 3.
- Zhang, M., Bu, Z., Jiang, M., Wang, S., Liu, S., Chen, X., Hao, J., Liao, W., 2019. The development of Hani peatland in the Changbai mountains (NE China) and its

- response to the variations of the East Asian summer monsoon. *Sci. Total Environ.* 692, 818–832.
- Zhang, H., Välimäki, M., Piilo, S., Amesbury, M.J., Aquino-López, M.A., Roland, T.P., Salminen-Paatero, S., Paatero, J., Lohila, A., Tuittila, E.-S., 2020. Decreased carbon accumulation feedback driven by climate-induced drying of two southern boreal bogs over recent centuries. *Glob. Chang. Biol.* 26 (4), 2435–2448.
- Zhang, C., Zhao, C., Yu, S.-Y., Yang, X., Cheng, J., Zhang, X., Xue, B., Shen, J., Chen, F., 2022. Seasonal imprint of Holocene temperature reconstruction on the Tibetan Plateau. *Earth Sci. Rev.* 226, 103927.
- Zhou, W., Zheng, Y., Meyers, P.A., Jull, A.J.T., Xie, S., 2010. Postglacial climate-change record in biomarker lipid compositions of the Hani peat sequence, Northeastern China. *Earth Planet. Sci. Lett.* 294 (1), 37–46.
- Zibulski, R., Wesener, F., Wilkes, H., Plessen, B., Pestryakova, L.A., Herzschuh, U., 2017. C/N ratio, stable isotope ( $\delta^{13}\text{C}$ ,  $\delta^{15}\text{N}$ ), and *n*-alkane patterns of brown mosses along hydrological gradients of low-centred polygons of the Siberian Arctic. *Biogeosci* 14 (6), 1617–1630.